Modeling of atmospheric-coupled Rayleigh waves on planets with atmosphere: From Earth observation to Mars and Venus perspectives

Ph. Lognonné, F. Karakostas, L. Rolland, Y. Nishikawa

Modeling of atmospheric-coupled Rayleigh waves on planets with atmosphere: From Earth observation to Mars and Venus perspectives

Philippe Lognonné, Foivos Karakostas, Lucie Rolland, and Yasuhiro Nishikawa

Citation: The Journal of the Acoustical Society of America **140**, 1447 (2016); doi: 10.1121/1.4960788
View online: https://doi.org/10.1121/1.4960788
View Table of Contents: https://asa.scitation.org/toc/jas/140/2
Published by the Acoustical Society of America

Modeling of atmospheric-coupled Rayleigh waves on planets with atmosphere: From Earth observation to Mars and Venus perspectives

Philippe Lognonné[a] and Foivos Karakostas
Equipe Planétologie et Sciences Spatiales, Institut de Physique du Globe de Paris-Sorbonne Paris Cité, Université Paris Diderot, 75013 Paris, France

Lucie Rolland
Observatoire de la Côte d'Azur, Laboratoire Géoazur—Université de Nice Sophia Antipolis, Valbonne, France

Yasuhiro Nishikawa[b]
Equipe Planétologie et Sciences Spatiales, Institut de Physique du Globe de Paris-Sorbonne Paris Cité, Université Paris Diderot, 75013 Paris, France

(Received 30 December 2015; revised 14 June 2016; accepted 22 June 2016; published online 31 August 2016)

Acoustic coupling between solid Earth and atmosphere has been observed since the 1960s, first from ground-based seismic, pressure, and ionospheric sensors and since 20 years with various satellite measurements, including with global positioning system (GPS) satellites. This coupling leads to the excitation of the Rayleigh surface waves by local atmospheric sources such as large natural explosions from volcanoes, meteor atmospheric air-bursts, or artificial explosions. It contributes also in the continuous excitation of Rayleigh waves and associated normal modes by atmospheric winds and pressure fluctuations. The same coupling allows the observation of Rayleigh waves in the thermosphere most of the time through ionospheric monitoring with Doppler sounders or GPS. The authors review briefly in this paper observations made on Earth and describe the general frame of the theory enabling the computation of Rayleigh waves for models of telluric planets with atmosphere. The authors then focus on Mars and Venus and give in both cases the atmospheric properties of the Rayleigh normal modes and associated surface waves compared to Earth. The authors then conclude on the observation perspectives especially for Rayleigh waves excited by atmospheric sources on Mars and for remote ionospheric observations of Rayleigh waves excited by quakes on Venus. © *2016 Acoustical Society of America*. [http://dx.doi.org/10.1121/1.4960788]

[AGP] Pages: 1447–1468

I. INTRODUCTION

Rayleigh surface waves correspond to the largest amplitudes recorded on long period seismograms. They propagate in the vicinity of the Earth surface with maximum amplitude at a depth of about one-third of their wavelength. Like all seismic waves, they can be either represented as wave solutions of the gravity-elastodynamic equation, fitting the surface boundary condition, or as seismic rays bouncing the surface several times along their propagation; see Aki and Richards (1980). Even if most of the seismology textbooks ignore the atmosphere and consider that all the wave energy is reflected at the Earth free surface, Rayleigh surface waves generate therefore vertical oscillations of the Earth surface acting like a piston on the surrounding atmosphere and transfer a small fraction of their energy to the atmosphere.

The dynamic ground coupling between the interior of the Earth and the atmosphere is however quite simple. It is only related to the continuity on both sides of the Earth's surface of the pressure and vertical displacement. As a consequence, all surface vertical displacement and pressure changes induced by atmospheric gravity and acoustic waves will generate seismic waves inside the solid Earth and/or tsunamis or acoustic waves in the ocean while on the other side, all seismic waves (for the solid part) or tsunami and acoustic waves (for the ocean) exciting the atmosphere with surface pressure changes or vertical surface displacements will lead to atmospheric gravity or acoustic waves. Several observations have illustrated this coupling mechanism since the development of seismology by the end of the 19th century.

The first one consists in the observation of seismic signals associated to strong atmospheric sources. Among the first were the records performed at Irkutsk, in Russia, following the atmospheric explosion of a meteor or comet in Siberia on June 30, 1908 (Ben-Menahem, 1975). Similar signals were also recorded following the major nuclear explosions performed by the United States and the Soviet Union in the atmosphere, between 1945 and their limited interdiction in 1963. Apart many reports and studies concerning atmospheric waves, see the early papers of Yamamoto (1956, 1957), Hunt *et al.* (1960), Press and Harkrider (1962), Donn and Ewing (1962a,b), and Harkrider (1964) for more specific Rayleigh wave observations. Very recently, seismic

[a]Electronic mail: lognonne@ipgp.fr
[b]Also at: University of Tokyo, Tokyo, Japan.

signals were recorded following a large meteor atmospheric explosion over Chelyabinsk and are illustrated by Tauzin *et al.* (2013) among others. See Edward (2008) and Edwards *et al.* (2008) for general reviews on the seismic detection of meteors.

Other powerful atmospheric sources are the volcano explosions, and the most famous observations remain those following the Pinatubo eruption in 1991. By stacking 12 IDA stations during 12 h, Zürn and Widmer (1996) have shown that the signals recorded following the Pinatubo eruption showed selective excitation of Rayleigh surface waves around frequencies of 3.7 mHz, 4.44 mHz for the two main peaks and 5.2, 6.1, and 7.2 mHz, where mHz denotes 0.001 Hz. Many papers were published on the explanation of these unusual signals. Some have proposed a feedback regime between the atmosphere and the volcano (Widmer and Zürn, 1992; Zürn and Widmer, 1996). Others proposed the excitation of two atmospheric waves corresponding to gravity and acoustic waves, respectively (Kanamori and Mori, 1992; Kanamori *et al.*, 1994). Lognonné *et al.* (1998), Lognonné (2009), and Watada and Kanamori (2010) finally demonstrated that these signals can be explained through the resonance of the Rayleigh waves with the atmospheric tropospheric and mesospheric wave guide, resulting in a large Rayleigh wave atmospheric sensitivity at the observed selective frequencies.

The discovery of the continuous excitation of normal modes (Suda *et al.*, 1998; Kobayashi and Nishida, 1998a,b; Tanimoto *et al.*, 1998) has originally suggested a second example of coupling between the solid Earth and its atmosphere (Nishida and Kobayashi, 1999; Tanimoto and Um, 1999; Fukao *et al.*, 2002). The first interpretations proposed that the excitation is produced by the turbulences of the Earth's atmospheric boundary layer. The seasonal variations of the continuous excitation (Nishida *et al.*, 2000) were also supporting an atmospheric origin and a simplified theory was proposed by Tanimoto (1999). The most recent studies show however that the major part of the source of continuous excitation is located over the oceans (Tanimoto, 2005; Rhie and Romanowicz, 2004, 2006) and that infragravity waves over the continental shelves are much more efficient seismic sources for this process (Webb, 2007). The excitation by atmospheric sources remains however significant below 5 mHz (Nishida, 2013) and its signature is strongly supported by the larger excitation of the Rayleigh modes at 3.7 and 4.4 mHz known to have a relative energy 5 times larger than the other modes in the atmosphere (Lognonné *et al.*, 1998). This larger excitation cannot be explained by pressure sources at the bottom of the ocean (Nishida, 2014).

The third example of coupling is related to ionospheric perturbations after earthquakes, for which many observations were reported in the 1960s after large quakes in Alaska or Japan (Yuen *et al.*, 1969; Weaver *et al.*, 1970; Leonard and Barnes, 1965; Davis and Baker, 1965). Two propagating paths can be considered. The first is mostly an acoustic atmospheric propagation of signals excited locally by the seismic source and propagating therefore mostly in the atmosphere up to a few thousand kilometers (Astafyeva *et al.*, 2009). The second on which we focus here is associated to seismic propagating waves finishing their path by an upward propagation in the atmosphere. Such signals can either be observed near a seismic source or at teleseismic distances. Only the seismic waves with frequencies larger than the acoustic cutoff frequency of about 3.7 mHz can however propagate upward and can reach the ionosphere, while those below the acoustic cutoff are damped rapidly with altitude. Due to the conservation of the momentum flux, these waves have their amplitude growing with altitude as the inverse of the square root of the density, before being affected by viscous and other attenuation processes and vanishing. Signals have been widely observed either through Doppler sounders or global positioning system (GPS) signals. For Doppler observations, Artru *et al.* (2001) have shown that the ground amplitude might be amplified by a factor of 50 000 when it reaches an altitude of 200 km. Typically, the detection threshold for atmospheric perturbations is about 10 m/s at 200 km (which generated, for example, a Doppler effect on the order of 3×10^{-8}). Such signal can therefore be detected for ground velocities down to about 0.2 mm/s, which allows to detect the surface waves of very large quakes at very large distances: 9000 km for Tohoku recorded with a Doppler sounder in Czech republic by Chum *et al.* (2012) and more than 14 000 km for a quake in New Ireland recorded in France by Artru *et al.* (2004). New generation high frequency (HF) sounders are now able to monitor such signals for quakes larger than 6.5 in moment magnitude (Artru *et al.*, 2004) and signals have also been observed by over-the-horizon systems, including for the R2 Rayleigh wave of the Ms = 8.6 Sumatra Earthquake in 2005, which reached France after about 30 000 km of distance (Occhipinti *et al.*, 2010). On both systems, Rayleigh wave signatures have furthermore been observed up to 20 s periods (Bourdillon *et al.*, 2014; Occhipinti, 2015).

GPS observations started with the pioneering work of Calais and Minster (1995). They have now reached maturity through the development of dense permanent high-rate GPS networks, enabling multiple observations and even wavefront imaging. See, among others, Ducic *et al.* (2003) and Rolland *et al.* (2011a). Last but not least, the very large Rayleigh waves generated by the Tohoku-Oki $M_w = 9.1$ earthquake of March, 2011 were of course observed not only by GPS (Maruyama *et al.*, 2012; Rolland *et al.*, 2011a) but also through their drag effect on the GOCE satellite, the latter orbiting at about 225 km of altitude (Garcia *et al.*, 2013).

The main goal of this paper is to present atmospheric Rayleigh waves in a comparative approach between Earth, Mars, and Venus and to discuss the perspective of atmospheric coupling of Rayleigh waves on other planets than Earth. We therefore first recall the theory able to take into account these coupling effects by an explicit calculation of the normal modes of the solid part of any planet model with a realistic atmospheric model, following the theory developed by Lognonné *et al.* (1998). This is first done for Earth and then for Mars and Venus, in the latter case taking into account the specific attenuation processes in the atmosphere of these planets associated to their CO_2 atmosphere. We then show several applications of this theory for the modeling of observed signals on Earth, or predicted signals on Mars and

the Moon: the first one, for Earth is the analysis of the Pinatubo eruption and of the recent Chelyabinsk explosion, which can be foreseen as examples of excitation of the solid Earth with sources in the atmosphere. The second is for Venus with the prediction of the amplitude of surface waves in the ionosphere. We conclude by a discussion on the perspective to detect from Venus orbit these signals for future orbital missions and to detect on Mars Rayleigh waves generated by atmospheric sources.

II. NORMAL MODE THEORY: BRIEF DESCRIPTION

Seismology is most of the time assuming that the surface of the Earth or planets with atmosphere is a free surface where the pressure forces are set to zero. This assumption is therefore used most of the time in the computation of the Rayleigh modes, which are the normal modes corresponding to the fundamental branch of surface waves. The latter is done by finding the fundamental eigen-solutions of the linearized elastodynamic equation, which in the non-rotating case can be written in a general Eulerian form and in the frequency domain as

$$\omega^2\mathbf{u} = \mathbf{A}(\mathbf{u}) = -\frac{1}{\rho}(\nabla\cdot(\mathbf{T}_{\text{elastic}} - \mathbf{u}\cdot\nabla\mathbf{T}_0) - \text{div}(\rho\mathbf{u})\mathbf{g} - \rho\nabla\Phi_{E_1}), \quad (1)$$

where ω is the angular frequency, $\mathbf{u}$ is the displacement vector, ∇ is the spatial derivative operator, ρ is the unperturbed density, and $\mathbf{T}_{\text{elastic}}$ is the stress departure from equilibrium. g is the gravity and Φ_{E_1} is the mass redistribution potential and where the equilibrium stress $\mathbf{T}_0$ is the solution of

$$\nabla\cdot\mathbf{T}_0 + \rho\mathbf{g} = 0\,. \quad (2)$$

Relation (1) defines the gravito-elastic operator $\mathbf{A}(\mathbf{u})$. This relation applies to either the liquid, solid part of the planet or the gaseous part of its atmosphere. The only difference is found in the constitutive relation of the elastic stress $\mathbf{T}_{\text{elastic}}$. In the solid parts, a symmetric stiffness tensor is generally used, which gives

$$\mathbf{T}^{ij}_{\text{elastic}}(\mathbf{r},t) = C^{ijkl}D_k u_l(\mathbf{r},t)\,. \quad (3)$$

In the fluid parts (either liquid or gaseous) and for adiabatic perturbations, we have $C^{ijkl} = \kappa g^{ij}g^{kl}$, where κ is the adiabatic bulk modulus and g^{ij} is the metric tensor, equivalent to the Kronecker symbol in Cartesian coordinates (g^{ij} is non zero and equal to 1 for $i=j$ only). In addition, solutions of the equation must also fit all continuity relations related to the continuity of stress and displacement on all solid/solid discontinuities, and of stress and vertical displacement on all solid/fluid or fluid/fluid discontinuities.

Normal modes $\mathbf{u}$ with associated normal frequency ω are the solution of these equations which in addition fit the upper boundary condition. For an upper liquid/solid interface, these lead to continuity of the vertical displacement and of the radial component of the stress, the latter vanishing at a free surface. See Takeuchi and Saïto (1972) and Woodhouse and Dahlen (1978) for more details on the background, and Lognonné *et al.* (1998) and Lognonné and Clévédé (2002) for specific details in the whole Earth case, i.e., with a solid and atmospheric part.

Resolution of these equations with Earth models with atmosphere having on their top a free surface can be done with the freely available MINEOS software (Master *et al.*, 2014), even if the latter software was originally not made for that purpose. Figure 1 shows typical results in terms of normal mode's frequencies for the PREM model (Dziewonski and Anderson, 1981) and a typical Earth atmosphere model, here the MSISE atmospheric model (Picone *al.*, 2002). While this approach solves correctly the continuity of vertical displacement and pressure at the Earth's surface, it is however far to be satisfactory due to the upper top free surface boundary condition and produces an artificial trapping of the waves between the Earth's surface and the top of the atmosphere.

The atmosphere is indeed such that no specific boundary can be defined, due to the exponential decay of the density. In addition vertically propagating waves or normal modes with frequency above the atmospheric acoustic cutoff are not reflected when propagating upward at high altitude and loose at these height their energy due to viscosity and other attenuation or non-linear effects. Above the acoustic cutoff, non-vertical acoustic waves can nevertheless be reflected in the stratosphere or thermosphere, especially when interacting with wind, leading to long distance propagating infrasounds.

In order to take into account these effects, it is first necessary to use a radiative boundary condition instead of the usual free surface boundary condition. Following Unno *et al.* (1989) and Watada (1995), this is made by assuming a local dependence of the modes at the top of the atmosphere as r^λ, where r is the planetary radius. As shown by Lognonné *et al.* (1998), each eigenfrequency ω determines two values for λ, respectively, associated to modes with upward and downward propagating energy. As proposed by Lognonné *et al.* (1998), the eigen-frequencies and associated eigen-modes can then be solved with a variational method which uses a basis of test functions, found by mapping the normal modes with free surface toward functions verifying explicitly the radiative boundary condition. Other techniques for the computation of the normal modes, based on propagators, have also been developed (Kobayashi, 2007; Watada and Kanamori, 2010).

Due to the decreasing density (and associated bulk modulus), it is also necessary to take, at higher altitude, above 100 km, viscous and possibly other attenuation effects. The typical frequency domain of the Rayleigh waves associated to atmospheric perturbations is from 1 to 50 mHz. In this range, viscous dissipation is expected to be important above 100 km height (Pitteway and Hines, 1963). The viscous stress tensor can be expressed by

$$\mathbf{T}'_{ij} = i\omega\mu_{\text{vis}}\left(\frac{\partial u_i}{\partial x_j} + \frac{\partial u_j}{\partial x_i} - \frac{2}{3}\delta_{ij}(\nabla\cdot\mathbf{u})\right). \quad (4)$$

Here, u_i is the ith component of displacement and μ the dynamic viscosity. This is a second order, frequency-dependent term that can be introduced in the variational process described, as described by Artru *et al.* (2001). Other

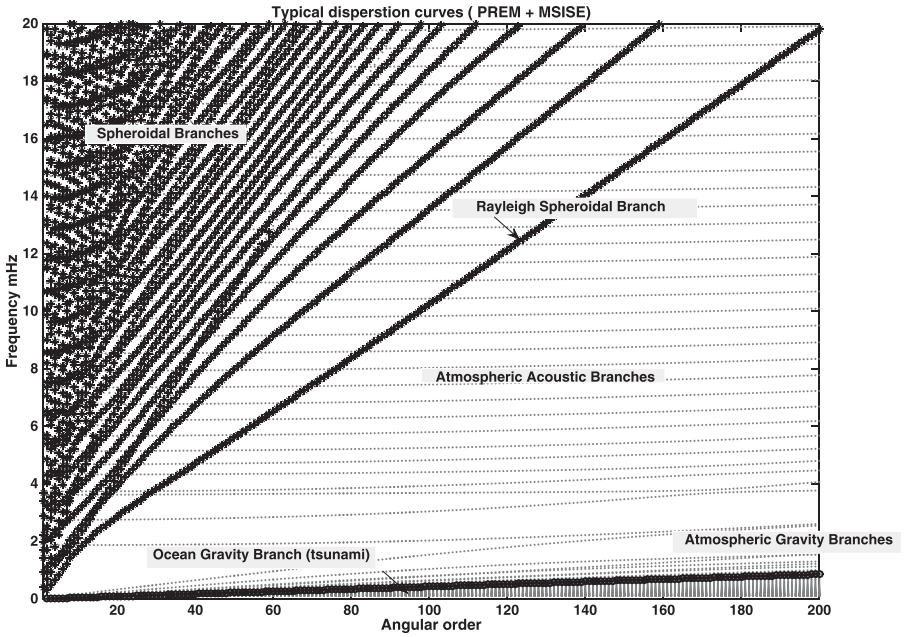

FIG. 1. Earth normal mode frequencies obtained for the Normal modes of Earth with PREM and the MSISE atmospheric model. These eigenfrequencies, computed with an atmosphere of 400 km of altitude with a free surface at the top of the atmosphere correspond to the basis of test functions used for the computation of normal modes with attenuation and radiation boundary condition (Lognonné *et al.*, 1998). Although the top boundary limit is not realistic, the frequencies of the trapped atmospheric normal modes are relatively well estimated, especially for the fundamental and first overtone of the acoustic and gravity modes and for the Lamb modes trapped on the Earth's solid/atmosphere surface. It also shows the different types of modes in a complex Earth or telluric planet: spheroidal modes, including the Rayleigh fundamental branch, atmospheric acoustic and gravity modes and for Earth, and tsunami gravity modes for 3 km depth ocean. The resonances of the Rayleigh waves are typically found at the frequencies corresponding to the fundamental and two first overtones. See another example in Lognonné & Clévédé (2002) with a different atmospheric model.

effects, such as molecular relaxation and heat transfer can be incorporated in the expression of the bulk modulus which then is not only imaginary but also frequency dependent. This will be particularly important for Mars and Venus.

Figures 2–5 show the results of Rayleigh normal modes computation for the Earth. These modes will be used later for computing seismograms recorded for the Chelyabinsk atmospheric meteor. Models with an ocean, such as those obtained from the PREM model, can be found in Lognonné and Clévédé (2001). In both cases, the main perturbations, for the spheroidal normal modes are found in the amplitude of normal modes rather than in the frequency or quality factor (whose perturbations are very small). Two regimes for the fundamental spheroidal modes are found: below the atmospheric cutoff, of about 3.70 mHz, the modes are trapped near the surface with an exponential decay of their amplitude with altitude. Above this frequency, modes propagate upwards.

Figure 2 shows the fraction of the energy of Rayleigh modes in the atmosphere. We have three resonances corresponding to those of the Rayleigh modes with the frequencies closes from the fundamental (3.70 mHz), first (4.30 mHz), and

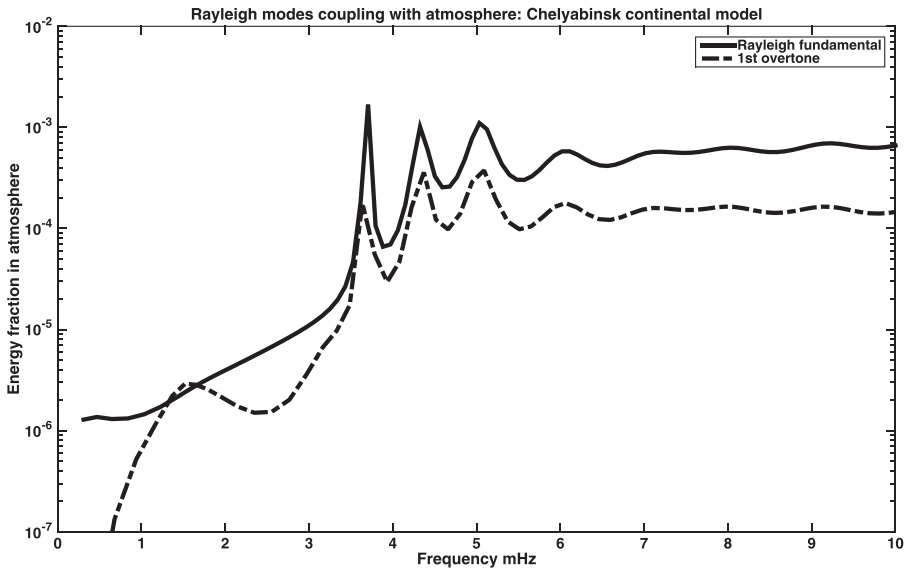

FIG. 2. Relative fraction of the energy of the Rayleigh normal modes and first spheroidal normal modes in the atmosphere. The three resonances have frequencies closest from the fundamental (3.70 mHz), first (4.30 mHz), and second (5.0 mHz) acoustic overtones and correspond to the crossing of the Rayleigh dispersion branch with these acoustic branches. The Rayleigh modes are those corresponding to the continental model beneath Chelyabinsk, with the MSISE atmosphere model at the local time and location of the meteor explosion.

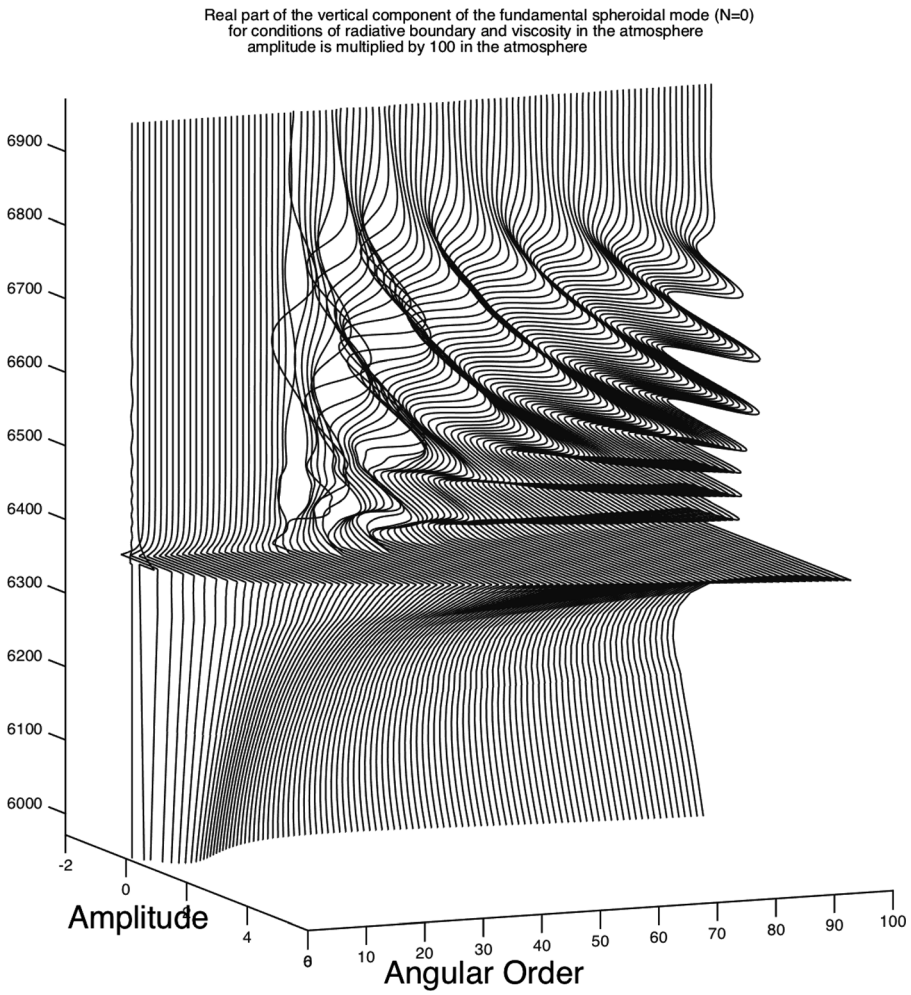

FIG. 3. Real part of the vertical amplitude of the solid spheroidal fundamental normal modes in the upper mantle and atmosphere. Modes are up to angular order 100. The amplitudes shown are multiplied by $\sqrt{\rho}$, where ρ is the density and multiplied by 100 in the atmosphere. Note that modes with angular orders lower than $\ell = 29$ have a frequency lower than the atmospheric cutoff and have an exponentially decreasing amplitude with altitude. Modes with angular orders above $\ell = 29$ have contrary oscillating amplitudes in the atmosphere. The resonances shown in Fig. 2 appear with larger amplitudes in the stratosphere.

second (5.03 mHz) acoustic overtones. These modes are the most sensitive to the atmospheric coupling and have 0.1%–0.2% of their energy in the atmosphere. The exact frequency and shape of the resonance depends on the atmospheric model. Note also that the first resonance is wider than the fundamental one and the second wider than the first one. For such frequencies and angular orders, the corresponding acoustic first and second overtones are indeed less efficiently trapped in the stratospheric wave guide (see Fig. 10) and have decreasing quality factors: slightly more than 100 for the fundamental acoustic but only about 20 and 5 for the first and second acoustic harmonics, as shown by Lognonné *et al.* (1998) who also provides the amplitudes of these acoustic modes with altitude. The harmonics indeed escape this waveguide through a tunneling effect and then loose progressively their energy by upward radiation (Francis, 1973). Rayleigh waves due to their much larger horizontal phase velocity are obviously much less trapped. Their upward propagative character is found in Fig. 4 for all Rayleigh waves above the atmospheric cutoff of 3.70 mHz which are all characterized by real and imaginary amplitudes in quadrature above the stratosphere. We finally show the fraction of the energy in the atmosphere for the first spheroidal overtone. It also has resonances at the same frequencies, but the coupling with the atmosphere is weaker, with 5 times less energy in the atmosphere.

The other figures show the normal mode amplitudes, as a function of depth or altitude. Below the atmospheric cutoff frequency (about 3.68–3.70 mHz as the exact frequency depends on the atmospheric model and therefore on the local time, latitude, and season), the atmospheric part of the mode is trapped and decreases exponentially with altitude. At higher frequencies in contrary, the energy propagates upward. This leads to beating amplitudes, with the real part and the imaginary part in quadrature. Figure 2 provides the real part and Fig. 4 the imaginary part. Note on Fig. 3, showing the horizontal amplitude of the Rayleigh modes, the large amplitude at the 3.68 mHz resonance and at 4.40 mHz, corresponding to the resonance of the Rayleigh modes when the dispersion branch cuts the fundamental acoustic and first overtone. For more details see Lognonné *et al.* (1998) and Watada and Kanamori (2010). Figure 5 shows comparable results for the first overtone of the spheroidal modes. All modes can be computed with this approach. But the higher order overtones show a much weaker coupling with the atmosphere as compared to the Rayleigh waves.

III. SEISMIC SOURCES AND SEISMOGRAMS: THEORY

As shown in Sec. II, normal modes can be computed for a complete Earth or planet model. The normal mode summation techniques can then be also applied for the computation of seismograms, wherever is the source (i.e., in the atmosphere or in the solid Earth) and wherever is the observation (i.e., on

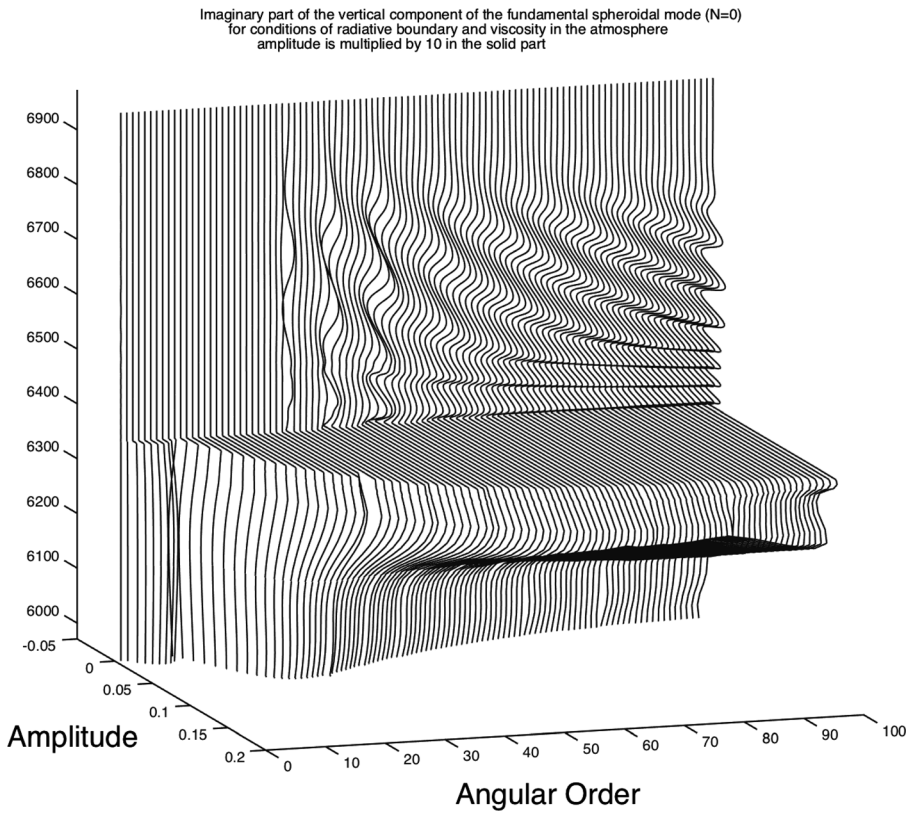

FIG. 4. Imaginary part of the vertical amplitude of the solid spheroidal fundamental normal modes in the upper mantle and atmosphere. Modes are up to angular order $\ell = 100$. The amplitudes shown are multiplied by $\sqrt{\rho}$, where ρ is the density and multiplied by 10 in the solid part. Note the much larger amplitude of the Normal modes in the atmosphere as compared to the solid part. Amplitudes of the normal modes in the atmosphere are in quadrature with respect to their real parts, indicating the upward outgoing energy associated to the leaky characters of the normal modes.

the solid surface with a seismometer or from the atmosphere or ionosphere with remote techniques).

For a source in the solid Earth, it can as usual be expressed with a Moment tensor and we refer to Lognonné and Clévédé (2001) for the complete expression. For a source in the atmosphere, Lognonné *et al.* (1994) have shown that the generalization of the concept of stress glut can be done. We recall here the demonstration. Let us consider the nonlinear equation of momentum conservation, written in the form

$$\partial_t(\rho\,\dot{\mathbf{u}}) = -\nabla p_{\text{true}} - \nabla\cdot(\rho\dot{\mathbf{u}}\dot{\mathbf{u}}) + \rho\mathbf{g}, \tag{5}$$

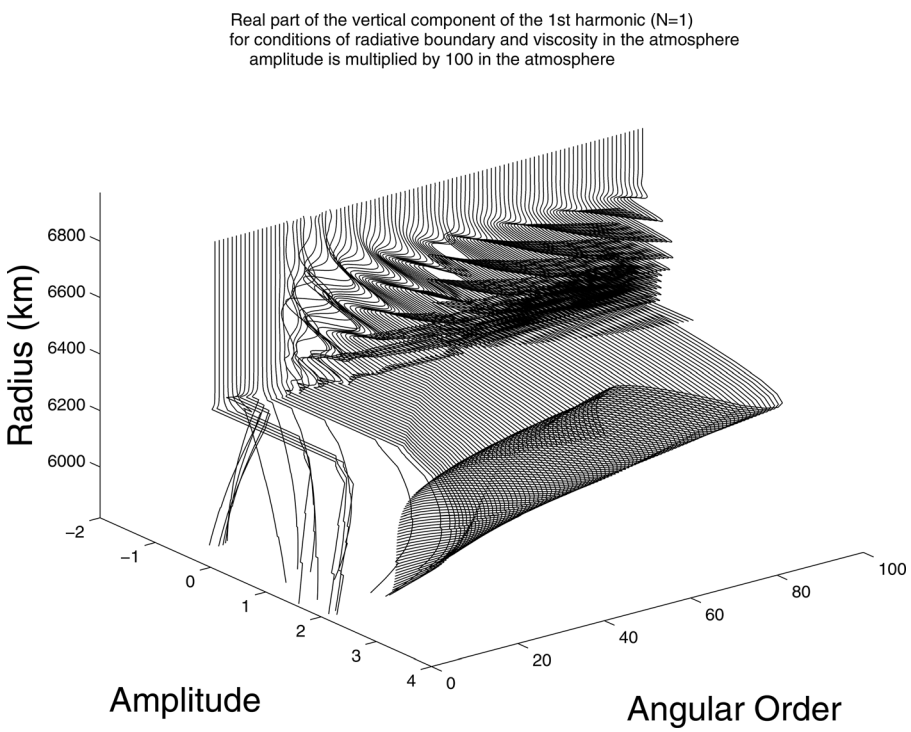

FIG. 5. Real part of the vertical amplitude of the solid spheroidal first overtone normal modes in the upper mantle and atmosphere. Modes up to angular order $\ell = 100$. The amplitudes shown are multiplied by $\sqrt{\rho}$, where ρ is the density and multiplied by 100 in the atmosphere. The same features as the fundamental are found for the exponentially decay with altitude below the atmospheric cutoff and the oscillating character above, as well as the resonances for frequencies indicated in Fig. 2.

where ρ is the density, $\mathbf{u}$ is the displacement with respect to the equilibrium position, $\dot{\mathbf{u}} = \partial_t \mathbf{u}$ is the velocity, p_{true} is the pressure, and where $\mathbf{g}$ is the gravity, given by the additional equation

$$\nabla \cdot \mathbf{g} = -4\pi \mathcal{G} \rho. \tag{6}$$

This expression is the one valid in the atmosphere. On the other hand, let us take the equation governing linearized seismology with self-gravitation

$$\partial_t(\rho\, \dot{\mathbf{u}}) = -\nabla p_{\text{Hooke}} + \mathbf{f}, \tag{7}$$

where the atmospheric force is $\mathbf{f}$, the model of Hooke pressure is defined as $p_{\text{Hooke}} = -\kappa \nabla \cdot \mathbf{u}$, and where $\kappa = \gamma \text{p}$ is the bulk modulus of the fluid. The difference between the two equations allows us to express the excitation force, which is given by

$$\mathbf{f} = -\nabla \cdot \mathbf{\Pi}, \tag{8}$$

where the momentum flux-glut tensor $\mathbf{\Pi}$ is the difference between the model momentum tensor, based upon Hooke's law and the true incremental momentum tensor. Here $\mathbf{\Pi}$ is given by

$$\mathbf{\Pi}_{ij} = (\text{p}_{\text{true}} - \text{p}_{\text{Hooke}})\delta_{ij} + \rho \dot{u}_i \dot{u}_j, \tag{9}$$

where δ_{ij} is the Kronecker symbol. The normal mode summation techniques (Lognonné, 1991) can now be used. Note that the theory must take into account anelasticity, both related to the attenuation in the solid Earth and to the energy escape related to the radiative boundary condition. We finally obtain

$$\mathbf{u}(t, \mathbf{r}_s) = \sum_{k>0} \Re e \left(\frac{1}{i\sigma_k} \int_0^t dt' M_k(t') e^{i\sigma_k (t-t')} \mathbf{u}_k(\mathbf{r}_s) \right), \tag{10}$$

where $\mathbf{r}_s$ is the receiver/station location, index k denotes a given mode with quantum numbers ℓ, m, n, σ_k, and $\mathbf{u}_k$ are the normal frequency and normal mode, respectively, associated to the index k and where the source term $M_k(t')$ is given by the source integrated over the whole source volume and is expressed by

$$M_k(t) = \int dV\, \Pi_{ij}(t) \nabla^i v_k^j, \tag{11}$$

where $\mathbf{v}_k$ is the dual normal mode. Depending on the integration volume, this expression can be used either for global scale atmospheric sources, such as those related to the continuous excitation of normal modes or for local, explosive sources, as illustrated by Lognonné *et al.* (1994) for the Shoemaker-Levy 9 impact on Jupiter.

IV. SEISMIC SOURCES AND SEISMOGRAMS: APPLICATION ON EARTH

No data have yet been collected for telluric planets other than Earth. Before providing the perspectives for Mars and Venus, we will therefore illustrate the theory described above with two examples, respectively, associated to ground observations of atmospheric sources and to atmospheric/ionospheric observations of quakes.

A. Atmospheric seismic source and ground observations

The importance of the atmospheric properties of Rayleigh waves excitation by atmospheric processes was mostly illustrated with the analysis of the Pinatubo seismic data, as this eruption was strong enough to excite the lowest frequency normal modes, below 5 mHz. As noted by Zürn and Widmer (1996), large low-frequency seismic signals were indeed detected by the World-wide Seismic Network after the eruption of the Pinatubo volcano, on June 15, 1991. The spectrum of these signals was characterized by 2 peaks, at 3.68 and 4.44 mHz. Figure 6 shows these signals at several of the Global Network (Geoscope and Iris) in both time and frequency domains. The resonance frequencies correspond to the trapped waves in the atmospheric waveguide, i.e., the two first horizontal branches of acoustic modes appearing on Fig. 1 and generating the large Rayleigh wave coupling resonance with atmosphere seen in Fig. 2. This selective excitation of a few Rayleigh normal modes close from atmospheric resonances is the key signature of an atmospheric source compared to internal ones, such as quake or explosion at depth, which excite all the Rayleigh normal modes up to the source cutoff frequency.

The sensitivity of the Rayleigh waves to the atmospheric coupling must be integrated for such atmospheric explosion in the attempt to inverse the seismic source. As shown by Lognonné (2009), reasonable and simple source amplitudes are found only for a source at 24–28 km of altitude, with most of the energy released at the time of the individual explosions and release of seismic moment are found near the reported date of the individual eruptions. These eruptions are associated to yields of about 4000 MT sec, corresponding to explosion releasing about 20 MT during blast times of about 200–500 s, which corresponds to the order of magnitude of the Pinatubo eruption, which released about 200 MT of energy in several explosions. In contrary, a complex mechanism at the source level is requested when the Rayleigh wave atmospheric coupling is not taken into account, as the source mimics then the specific excitation coefficients of the Rayleigh waves associated to resonances in the atmospheric structure.

Meteor disruption and their associated airburst are other possible atmospheric sources of Rayleigh waves, but are generally, due to their smaller energy, not exciting strongly the resonant normal modes. We illustrate here the results with the more recent Chelyabinsk event. On February 15, 2013, at 09:20:26 local time (UTC+6) a meteorite exploded in the atmosphere above the urban region of Chelyabinsk, Russia. With a surface wave magnitude of Ms = 3.7, calculated by the amplitude of Rayleigh wave displacement on the vertical component (Tauzin *et al.*, 2013), Chelyabinsk was the most important meteor event of the modern seismology era after the 1908 Tunguska event. However, given the quantity of available recordings at the stations of the Global

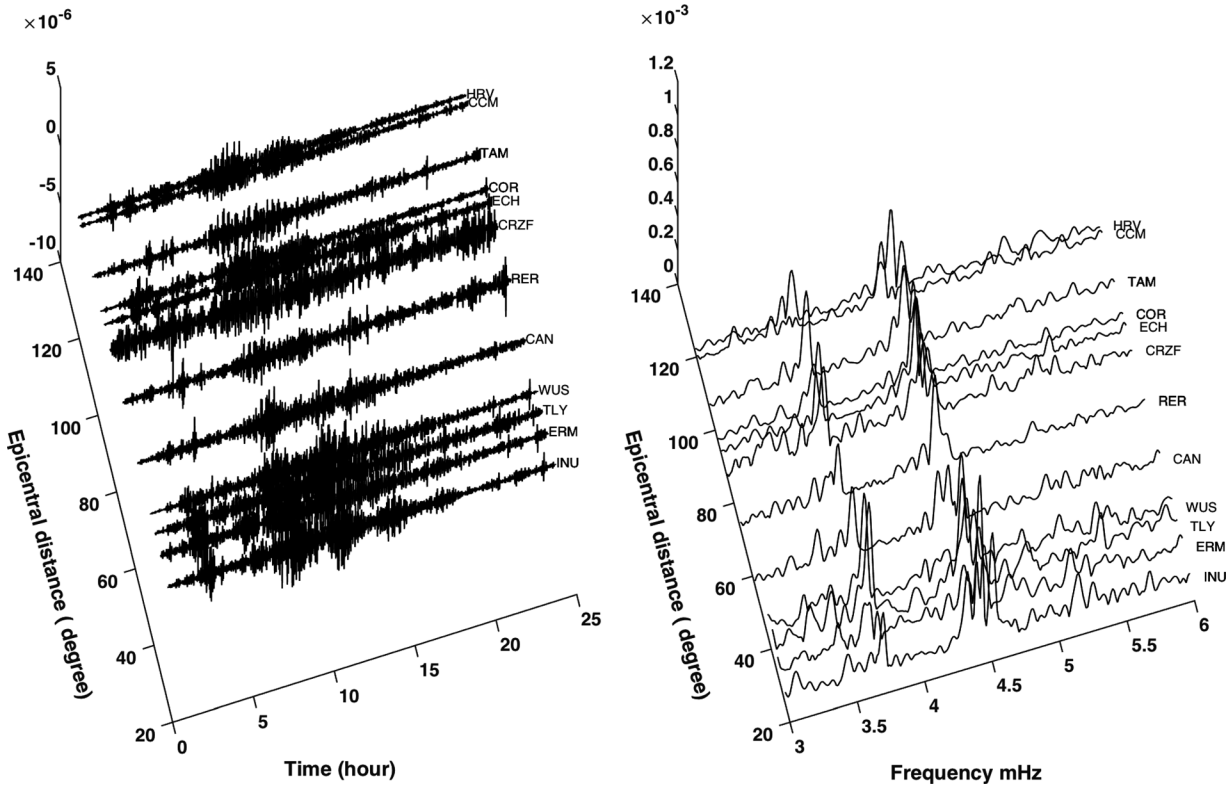

FIG. 6. Left, 1–8 mHz bandpassed data recorded after the Pinatubo eruption by several stations of the global network. Note two small quakes recorded on the data and originating from other sources as the Pinatubo region (an Ms = 6.1 quake from Causasus and a Ms = 6.3 quake from South Sandwich Islands, occurring, respectively, at 0059TU and 0113TU). Right, 12 h spectrum of the corresponding data, showing the 2 peaks of resonance.

Seismographic Network, as well as optical observations, the Chelyabinsk event offers unique data for modeling the signals with the air-coupled Rayleigh waves described above, which was not accounted for by Tauzin *et al.* (2013).

When a meteor enters the atmosphere of a planet, two kinds of shock waves are generated. The first is due to the friction of the impactor with the ambient atmosphere and generate a supersonic cylindrical blast, with the shape of a Mach cone of an angle of about 1°. The second is a spherical shock wave, generated by the fragmentation of the meteor, when the friction between the ambient atmosphere and the impactor is larger than the cohesive forces of the body. See more in ReVelle (1974). Therefore, a meteor can be modeled as a line atmospheric source followed by an explosion. The reconstruction of this mechanism will provide very important constraints on the strength of these seismic sources and serves as an important tool for calibrating these processes for planetary seismology and the estimation of the seismic source associated with airburst associated to Martian or Venusian impacts.

In order to understand the characteristics of Chelyabinsk atmospheric source, we used therefore the same methodology as above, but limited the moment release at a given altitude, assuming furthermore a constant value during a release time τ. Authors's future work will generalize this approach with an additional line source, where we will consider a sequence of point sources in the atmosphere, along the trajectory of Chelyabinsk super-bolide, provided, for example, by Borovička *et al.* (2013).

Like for Pinatubo, seismograms were again computed through a normal mode summation technique, but that time with a model corresponding to the *a priori* interior and atmospheric structure of the Chelyabinsk region. Normal modes were therefore calculated for a model of a complete Earth consisted by: (a) PREM (Dziewonski and Anderson, 1981) for Core and Lower Mantle, (b) a local Chelyabinsk model, provided by RSTT (Myers *et al.*, 2010) for upper mantle and crust, and (c) an atmospheric local Chelyabinsk model from the NRLMSISE-00 model with the corresponding location, local time, and Sun index F10.7.

Figure 7 illustrates the results on the inversion for a set of seismic stations located relatively close from the event. The obtained Moment is such that $M \times \tau = 3 \times 10^{16}$ Nms for an altitude of 17.5 km., which correspond to Moment magnitude given by $M_w = 5 - 2/3 \times \log_{10}(\tau)$. Further analysis will allow to constrain both the duration of the blast and the complexity of the atmospheric source, in a way comparable to the source function history shown for the Pinatubo eruption. The fit between observation and synthetic data for such a simple source is however already very satisfactory, and provides a second example of the validity of the air-coupled Rayleigh waves.

B. Quake seismic source and ionospheric Rayleigh waves observations

If our two first examples were on the excitation of Rayleigh waves by atmospheric sources, we illustrate here the detection, in the atmosphere, of Rayleigh waves generated by

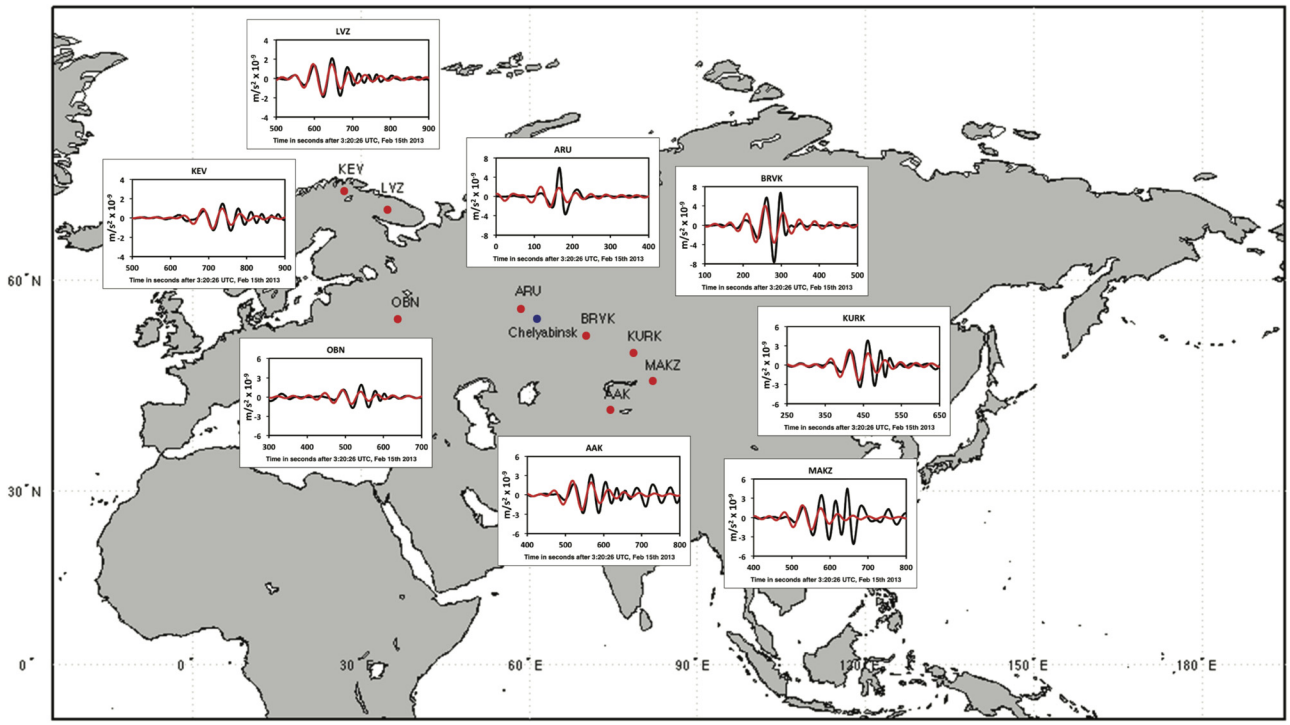

FIG. 7. (Color online) Observation and fit of the Rayleigh waves generated by the atmospheric source of the Chelyabinsk meteor. The obtained Moment is such that $M \times \tau = 3 \times 10^{16}$ Nms for an altitude of 17.5 km, which correspond to a Moment magnitude given by $M_w = 5 - 2/3 \times \log_{10}(\tau)$. Inversion of the moment has been done following the method used by Lognonné (2009) for the Pinatubo eruption.

quakes. Figure 8 illustrates several observations made at different altitudes, from ground up to the ionosphere, at 300 km of altitude. As discussed in Sec. I, the vertical neutral wind generated by the Rayleigh wave is amplified as a function of altitude, and the largest amplitudes are therefore found in the ionosphere.

Before the maximum of ionization and at height from 150 to 200 km, Doppler sounders provide very precise measurements of the vertical ionospheric velocity and are therefore instruments enabling broad frequency measurements, as illustrated by Artru *et al.* (2004) and Chum *et al.* (2012). The typical threshold for observation varies between Moment magnitude 6.5 to 7, and larger quakes provide high quality data, as illustrated by Maruyama *et al.* (2012) in ionograms recorded after earthquakes with seismic magnitude of 8.0 or greater and after the 2011 Tohoku-Oki earthquake, in particular, Maruyama and Shinagawa (2014).

But Doppler sounders remain complex systems and GPS systems have completely changed our view by providing access to very dense measurement systems, enabling the measurement of the Rayleigh waves in the range of 250 to 350 km of altitude. To correct the delay introduced by the ionosphere, GPS satellites use two frequencies (1.2 and 1.5 GHz). The derived ionospheric correction term is proportional to the amount of electrons on the GPS satellite to GPS receiver ray path, namely, the total electron content (TEC). See Lognonné *et al.* (2006) for a general description of the techniques and Occhipinti *et al.* (2013) and Ochipinti (2015) for recent reviews of TEC observations. Taking advantage of the dense GPS permanent network in California, Ducic *et al.* (2003) have monitored the first two-dimensional images of ionospheric perturbations related to the Rayleigh waves generated by an earthquake. The ionospheric fluctuations were observed about 10 min after the arrival, on the ground, of teleseismic Rayleigh surface waves generated by the 2002 Mw = 7.9 Denali earthquake (Alaska). This corresponds to the time needed by the atmospheric pressure wave forced by the piston-like effect of the ground vertical vibrations to propagate at sound speed up to the ionospheric sounding height, at about 300 km of altitude. As GPS satellites provide TEC measurements down to 10° of elevation, this experiment introduced a novel technique for mapping the Rayleigh waves group velocity above the ocean, offshore California. A three-dimensional image was even developed by Garcia *et al.* (2005), enabling the imaging of the Rayleigh waves between 200 and 500 km of altitude. A more recent example was following the Mw = 7.9 Gorkha earthquake in Nepal in 2015. Reddy and Seemala (2015) have performed measurements of Rayleigh wave local group velocities from their ionospheric counterparts over different places of the Indian subcontinent and have shown that these measurements are coherent with the values estimated by seismic tomography. These two examples show that the ionospheric observations of Rayleigh waves cannot only be used to detect waves and therefore quakes, but can also be used for measuring the speed of these waves and therefore providing structural information on the upper mantle of the planet. This of course will be of particular interest if applied to other planets than Earth.

If the phase or group velocity of the Rayleigh waves detection in the ionosphere is the same as those detected by seismometers at the surface, the amplitude of these ionospheric signals does depend on the atmospheric and ionospheric

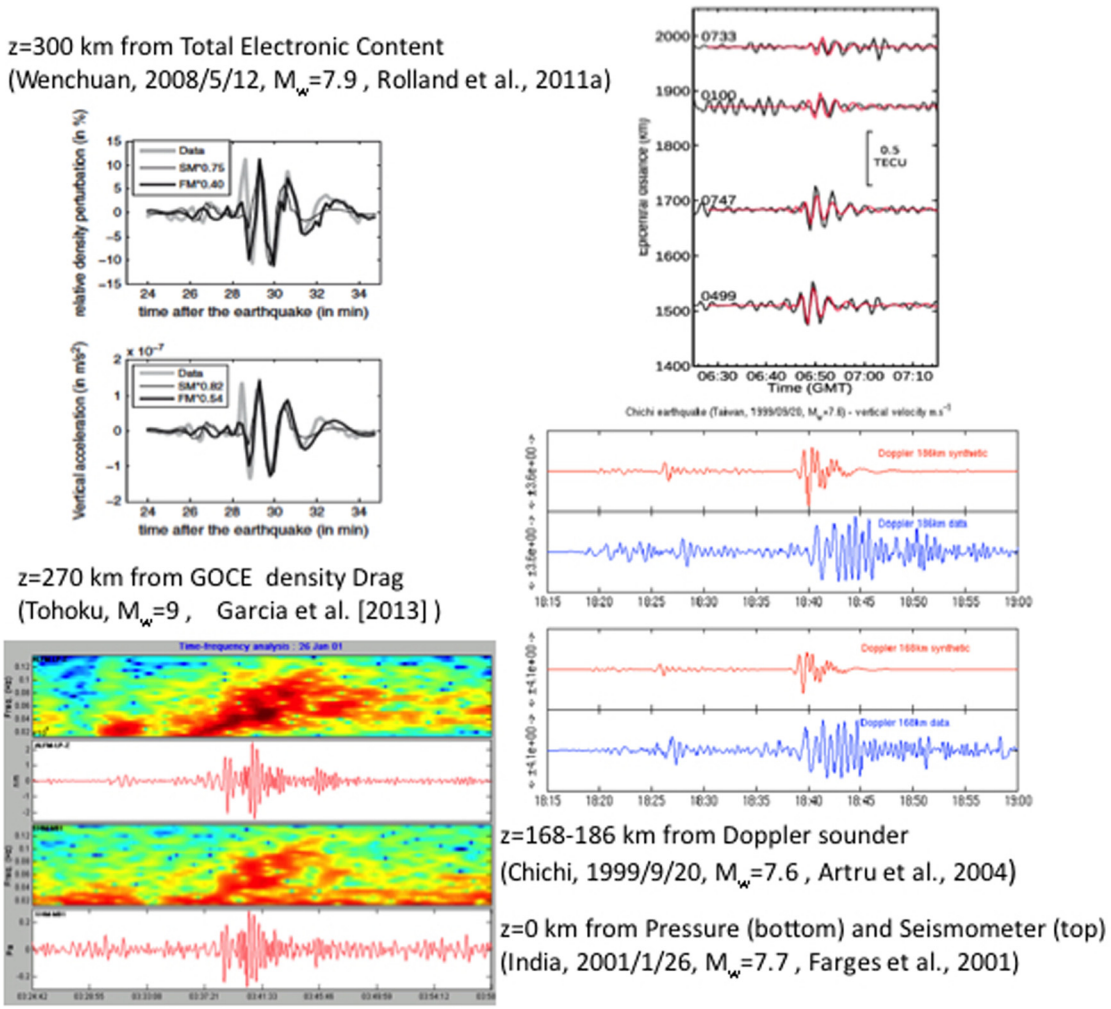

FIG. 8. (Color online) (a) Summary of atmospheric/ionospheric observations of seismic waves made at different altitudes and with different tools, from ground up to about 300 km of altitude. Pressure and seismometer observations made in Mongolia, for an Mw = 7.7 quake in India from the CEA monitoring station. The seismometer signal is shown in displacement, with 20 s Rayleigh surface waves peak amplitude of about 2 mm in amplitude, leading to pressure fluctuations of about 0.20 Pa. (b) Doppler sounder signals of the Chichi Taiwan earthquake, Mw = 7.6, recorded in France at altitude ranging from 165 to 185 km. These signals correspond to maximum vertical oscillations of the ionosphere of about 4 m/s. Adapted from Artru *et al.* (2004). (c) Drag observation generated by the Rayleigh waves of the Tohoku, 2011, Mw = 9 earthquake recorded at the altitude of the GOCE satellite. The amplitudes are about 15% of relative neutral density of the atmosphere. Adapted from Garcia *et al.* (2013). (d) Observed Slant TEC time series at far field of the Wenchuan earthquake (Mw = 7.9). The GPS GEONET stations are located in Japan, about 1500–2000 km east from the epicenter. The time series are filtered between 4 and 10 mHz, and the epicentral distance is indicated at the left of the figure. The 0.5 TEC amplitude corresponds to 1%–2% of the typical daily variation of the TEC and are associated to ionospheric velocity amplitudes of about 30 m/s of peak amplitude at 300 km altitude, generating local electron density variations of a few 10^{10} e/m^3. Adapted from Rolland *et al.* (2011b). In (b), (c), and (d), data are compared to synthetics computed through normal modes, the latter being, respectively, in black color for (c) and red for (b) and (d).

structure. Rolland *et al.* (2011b) have developed the solid Earth-atmosphere coupling scheme described and have added the ionospheric coupling and therefore the transfer of momentum from neutral atmospheric Rayleigh waves into electron density perturbations. This theory allows the reconstruction of the TEC fluctuations induced by Rayleigh waves. The coupling effects between the neutral and ionized atmosphere can then be modeled accurately by taking into account the *a priori* ionosphere structure and local geomagnetic field. The complete coupling appears to depend significantly on the local time and location, due to the conjugate effects of the atmosphere and ionosphere variabilities and on the magnetic field. Figure 9 shows the dependence of the coupling strength between Earth and atmosphere for the first resonant spheroidal modes on variable environmental parameters such as local time, season, latitude, and solar flux. We remark that the solar heating increases the coupling efficiency. More details on these observations, as well as on the observations of Rayleigh waves by TEC for other quakes can be found in Astafyeva and Heki (2009), Astafyeva *et al.* (2009), and Rolland *et al.* (2011b), among others.

V. MARS AND VENUS

Very few publications have been done on the strength of acoustic coupling between the Mars or Venus interior with their atmosphere. Kobayashi and Nishida (1998a,b) made the first estimation of the amplitude of the Mars and Venus continuous oscillations through a parametric comparison between Earth, Mars, and Venus. Garcia *et al.* (2005) made

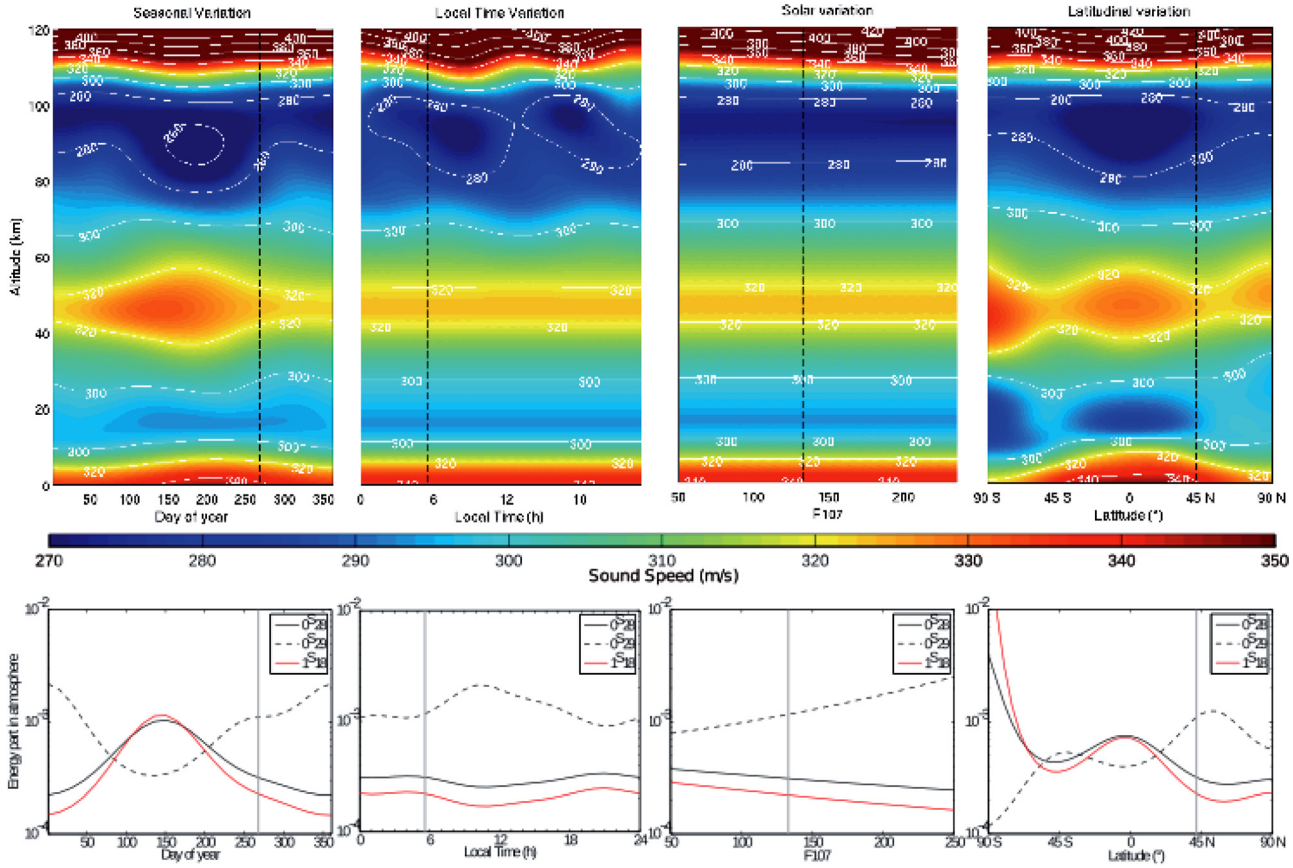

FIG. 9. (Color online) Variability of the Earths solid/atmosphere coupling as a function of local time, season (day of year), latitude, and solar flux F10.7. The part of the energy injected in the atmosphere is shown for the first resonating modes ${}_0S_{28}$, ${}_0S_{29}$, ${}_0S_{37}$, and ${}_1S_{18}$. Each vertical line corresponds to the reference model computed at the time and location of the 2003 Tokachi-Oki earthquake derived from the NRLMSISE-00 model. See more in Rolland *et al.* (2011b).

the first estimations on Venus for body wave amplitudes above the epicenter of quakes, while Lognonné (2005) and Lognonné and Johnson (2007) made those of remotely detected surface waves without considering attenuation processes.

We will extend below these precursor papers by a more careful modeling of the Rayleigh normal modes, accounting previously neglected attenuation effects and will precise the perspectives for future observations, with a special focus on the Venus remote detection in the ionosphere. We will also discuss in Sec. VI the perspective to detect, on Mars, Rayleigh waves excited by air-busts.

Although the physics of coupling remains the same, several major differences are found between Earth and Mars and Venus. Obviously, the first are the surface pressure and density, and therefore the acoustic jump between solid and atmosphere. With a density of about $2 \times 10^{-2}\,\mathrm{kg/m^3}$, Mars will have a much weaker, by a factor of 1/50 coupling than Earth while Venus, with its density of about $70\,\mathrm{kg/m^3}$ will have on the opposite a much larger coupling, by a factor of about 50 as compared to the Earth.

The second difference will be related to the atmospheric trapping of the modes and the associated frequency cutoff: the two planets do not have the Earth tropospheric-mesospheric acoustic channel. Consequently and in the absence of wind, the acoustic infrasounds are only trapped by the exponential decay of the atmospheric density. This effect is shown in Fig. 10, for the first 175 km of altitude for Earth, Venus, and Mars. The Earth atmospheric model is based on MSISE-00 (Picone *et al.*, 2002), the Mars model on Mars Climate Database atmospheric models (Forget *et al.*, 1999), and the Venus model on Venus GRAM model (https://software.nasa.gov/software/MFS-32314-1). For all three models, local time, seasonal, and latitudinal variations are expected. Wind of course will be important for the propagation of Mars and Venus infrasound over large distances as they can generate an acoustic waveguide not existing for a non-windy atmosphere. See, for the Earth, Mutschlechner and Whitaker (2009) for a review and Brissaud *et al.* (2016) for a recent modeling example. The wind effect is however much less important for the atmospheric part of Rayleigh waves, as they generate an almost vertical acoustic propagation in the atmosphere due to their very large horizontal phase velocity ($\simeq 3\,\mathrm{km\ s^{-1}}$). Wind is therefore neglected in this analysis, including in the above described confrontation with Earth data.

The last major difference will be associated to the CO_2 nature of the atmosphere, with differences in the acoustic velocities but more important in the attenuation processes. As this feature is unique for Mars and Venus compared to the Earth, we first describe it more in detail in Sec. V A.

A. Attenuation on Mars and Venus

As already described by Bass and Chamber (2001) and Williams (2001), molecular relaxation for Mars and Venus

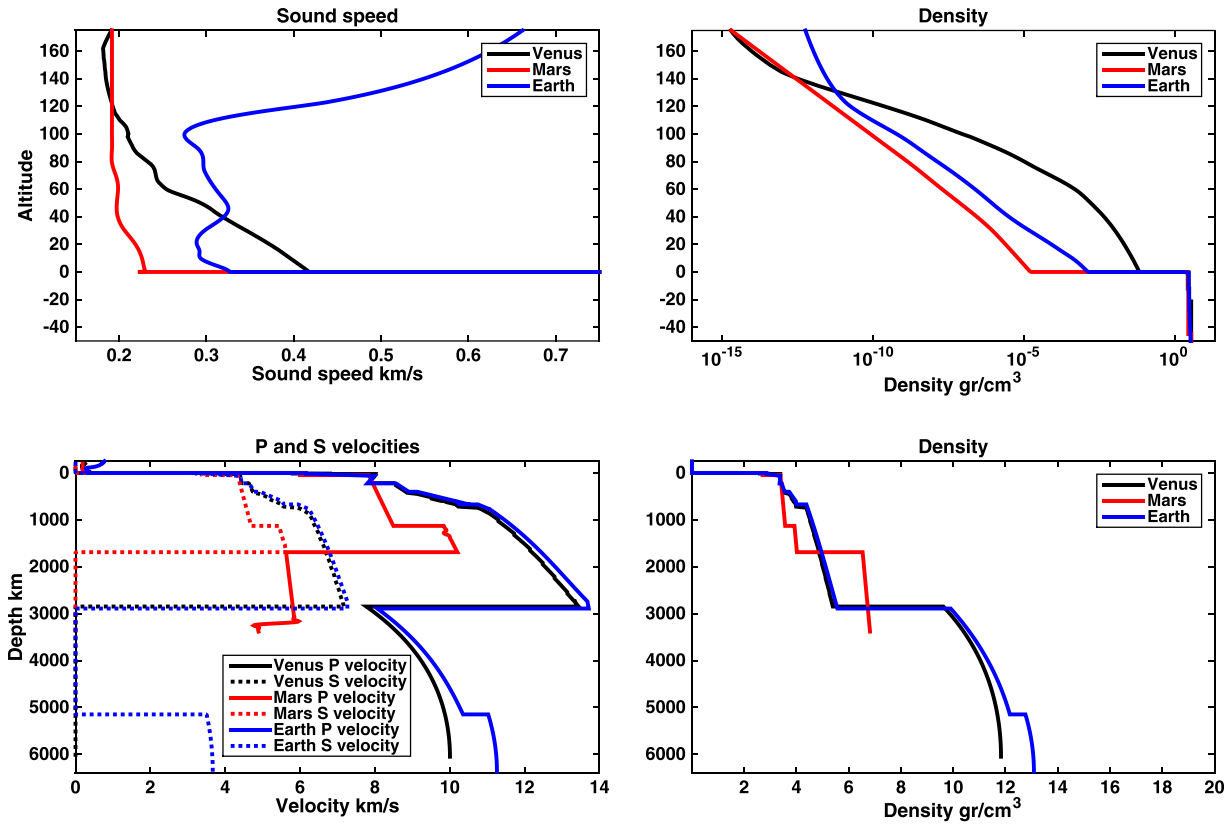

FIG. 10. (Color online) Comparison of the models used for Earth, Mars, and Venus. All solid models are based in some way of PREM, for better comparisons of the impact of atmosphere. Note the lack of an atmospheric low velocity zone as compared to Earth for both Mars and Venus, where the velocity mainly decreases with altitude. Rayleigh normal modes have their maximum sensitivity at one-third of their wavelength and will therefore have on Mars lower velocities than on Earth and Venus, mainly due to the reduced increase of pressure (and therefore seismic velocities) with depth.

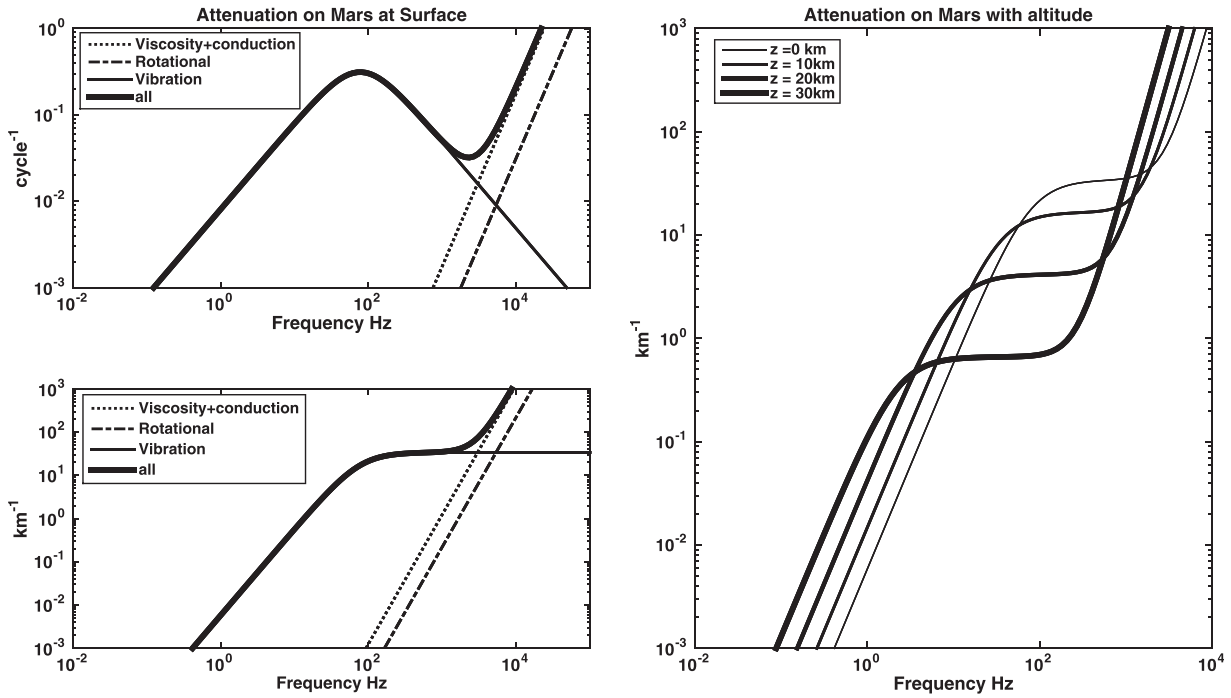

FIG. 11. Top left, attenuation factor per cycle and bottom left attenuation factor per kilometer for the Martian surface. The LMD Martian atmospheric model is used, providing a pressure of 8 mbar and temperature of 189 K at the surface. On the left panel, the attenuation factors are shown for the viscosity and conduction only (dotted line), the rotational relaxation only (dotted-dashed line), for the vibration only (thin continuous line), and for all attenuation (thick continuous line). On the right are the attenuation factors depicted for altitudes of 0, 10, 20, and 30 km with increasing line thickness.

is the largest source of attenuation for infrasounds contrary to Earth where this attenuation source is neglected.

Molecular relaxation can be modeled in normal modes and acoustic propagation processes by complex and frequency dependent heat capacity coefficients, which generates complex and frequency dependent bulk modulus or a complex adiabatic index. The complex bulk modulus must then be used in the resolution of the normal mode Eq. (3) for the expression of the stress tensor or need to be used as such in the acoustic equations. As normal modes are computed in the frequency domain, these sources of attenuation are however straightforward.

The quantification of the attenuation effect however can be more easily understood with the attenuation factor λ, which expresses the exponential decay of a plane wave in a homogeneous media, written as

$$u(s,t) = u_0\, e^{-\lambda s} e^{i\omega(t-s/c)}, \tag{12}$$

where c is the sound velocity, s and t are the propagation distance and time, respectively, and u_0 is the initial amplitude. The inverse of λ is therefore the distance for which the amplitude of the wave decreases by e and its kinetic energy flux decreases by $1/e^2 = 0.135$, about 1 order of magnitude. This attenuation factor is shown for the Martian condition in Fig. 11.

This attenuation is catastrophic on Mars in the audible bandwidth and for frequencies larger than a few tens of hertz, leading to a very large attenuation after a few kilometers of propagation as already noted by Bass and Chambers (2001) and Williams (2001). At long periods however, and especially in the range of Rayleigh waves (below 0.1 Hz), this attenuation is still relatively weak, with attenuation factors smaller or much smaller than 0.01 km^{-1}, which practically means small effects in the first 100 km of altitude on Mars and obviously much less on Venus for larger pressure and therefore density. Typically, we can expect therefore small effects from the atmospheric source to the ground in excitation processes or from the wave front to the ionosphere for observation. Our modeling approach is nevertheless fully accounting for the viscosity and molecular relaxation, and results for Mars and Venus are shown below.

B. Atmospheric coupling of Rayleigh modes and surface waves on Mars

We modeled Mars Rayleigh normal modes by using the MARS AR model (Okal and Anderson, 1978) an internal Mars model based on PREM. The atmospheric model used is derived from the LMD model. Both interior and atmospheric models are shown in Fig. 10 and the atmosphere was extended up to 200 km of altitude. Extension to a larger

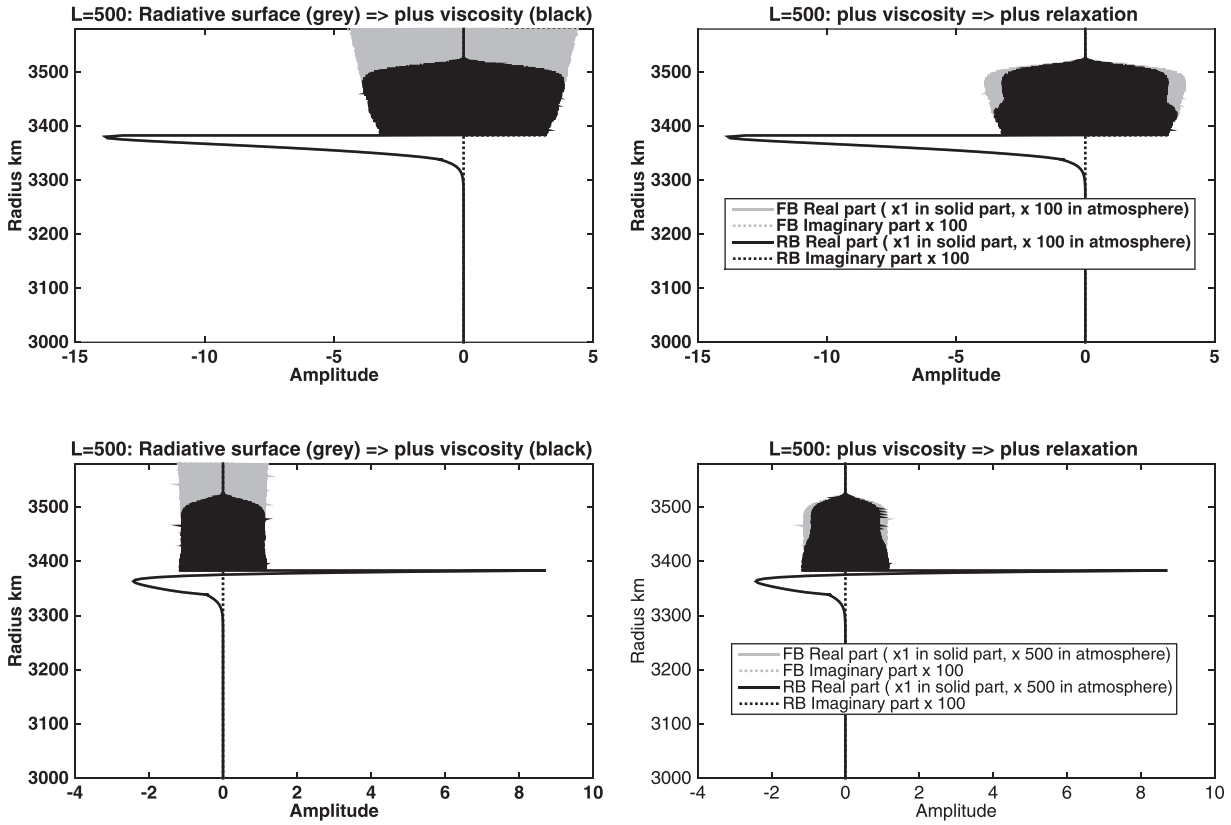

FIG. 12. Effect of the viscosity and of the molecular relaxation on the Martian Rayleigh normal mode with angular order 500, corresponding to periods of 13.7 s and therefore of regional surface waves. The two top figures are those providing the vertical displacement normalized with the density, while the two bottoms are for the horizontal density normalized displacement. Density normalization is made by multiplying the amplitude by $\rho(r)$ as for Fig. 3 which corrects the increase with altitude with respect to the scale height. The slight amplitude with radius above the Mars solid surface (for radius larger than 3383 km) is related to the decrease of the sound speed with altitude, as seen in Fig. 10. The left figures compare in gray the amplitudes without viscosity to those, in black, with viscosity. In both cases, the modes are computed with radiation boundary condition. Viscosity effects remain small until about 100 km of altitude in the atmosphere (3483 km radius) and lead to almost complete absorption of the waves in less than 20 km above these threshold heights.

altitude has been also made, and no significant differences on the mode amplitudes have been found in comparison.

Due to both the low surface density and CO_2 attenuation effects, Mars is the telluric planet where Rayleigh waves have their atmospheric amplitude vanishing at the smallest altitude, almost in the range of 150–200 km altitude, depending on the frequency. These attenuation effects are shown in Fig. 12 for a Rayleigh mode with angular order $\ell = 500$ corresponding to a period of 13.7 s. Note that in all these figures, the amplitude is scaled by the square root of the density. We note an almost complete attenuation of the mode at 120 km of altitude and significant effects of the molecular relaxation at altitudes of about 25 km, leading to about 20% amplitude reduction at 100 km altitude. The extension of the mode amplitude up to about 100 km seems nevertheless surprising as compared to Earth, as we start to see on Earth attenuation effects at about the same altitude, but much less severe above. In fact, and as a consequence of the larger scale height of Mars (about 11 km) than on Earth (8.5 km), the density ratio between Earth and Mars at 115 km altitude is only a factor of 4 and is therefore much smaller than on ground, where it is about 15 times larger. On Earth, however, amplitudes remains significant above 120 km, especially due to both the increase of the scale height in the thermosphere and to the larger sound speed which leads to a much less catastrophic attenuation above 100 km of altitude as the one observed on Mars and illustrated in Fig. 12. We see especially that this attenuation is comparable for all modes, including those with a frequency just above the acoustic cutoff.

An interesting feature, shown in Fig. 13 and found only on Mars, seems to be related to the large attenuation for altitudes larger than 100 km. Even if the molecular relaxation is large at the surface compared to viscosity, this is not the case anymore at these altitudes. As the density is decreasing with a height scale of about 8 km at 100 km, an increase by 10 of the viscosity occurs in about 20 km. For waves in the range of a few megahertz, such viscosity increase is made on a small fraction of the wavelength (with a sound speed of 200 m/s, 2 mHz waves will have a 100 km wavelength). Consequently, the large increase of viscous stresses may act as a reflecting boundary in the normal mode Eqs. (1)–(4).

The Mars atmosphere is such that the atmospheric cutoff frequency (about 2.2 mHz) is very close from those of waves with a wavelength of 100 km. This can be seen in Fig. 14, for the first oscillatory mode in the atmosphere with $\ell = 10$ and which shows one full wavelength before hitting the high dynamic viscous zone above 100 km altitude. Both this oscillatory mode and the mode just below the atmospheric cutoff ($\ell = 9$) are therefore in a resonance configuration with respect to the waveguide delimited by the interior-atmosphere boundary and the 100 km altitude transition to large dynamic viscosity. By examining the imaginary part of these modes, we furthermore see that the mode $\ell = 9$ is a non-propagating mode with a small imaginary part below 100 km while mode $\ell = 10$ has an onset of propagation with its imaginary part half away from quadrature, the latter being achieved for the mode with $\ell = 11$ which is therefore fully propagating upward. This resonance effect can be also seen when comparing the Rayleigh

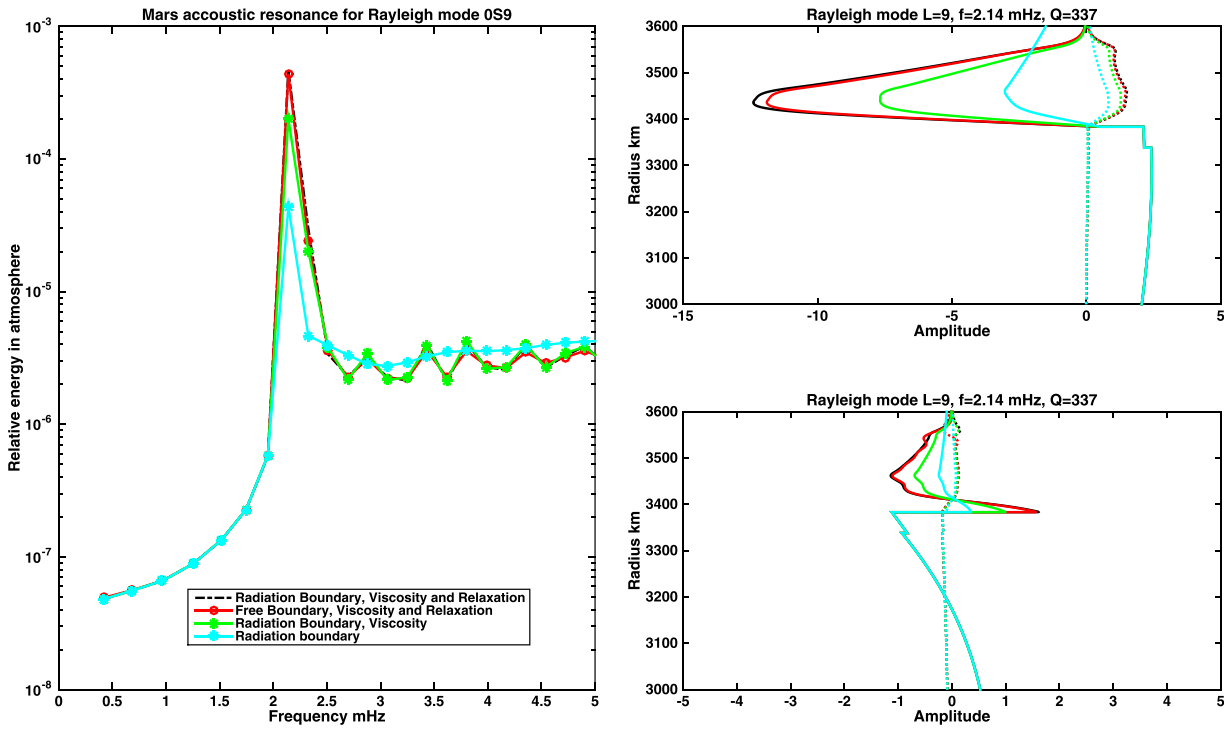

FIG. 13. (Color online) Right: Comparison of the vertical and horizontal amplitudes of the Rayleigh mode at resonance, corresponding to 0S9, with about 2.14 mHz. Two are without any attenuation and with radiation boundary (cyan curve) and with viscosity and radiation boundary condition (green). The two others are with relaxation and viscosity but with different boundary conditions: free surface boundary for the red curve and radiation boundary for the dotted black curve. The vertical axis is the planetary radius, with surface at 3383 km. Left: distribution of the relative atmospheric energy of the normal modes, as a function of frequency in the atmosphere, with the same color codes. Note that the two curves with relaxation almost superimpose on the left and have a small difference on the right, as most of the normal modes amplitude is canceled by the relaxation processes before reaching the boundary.

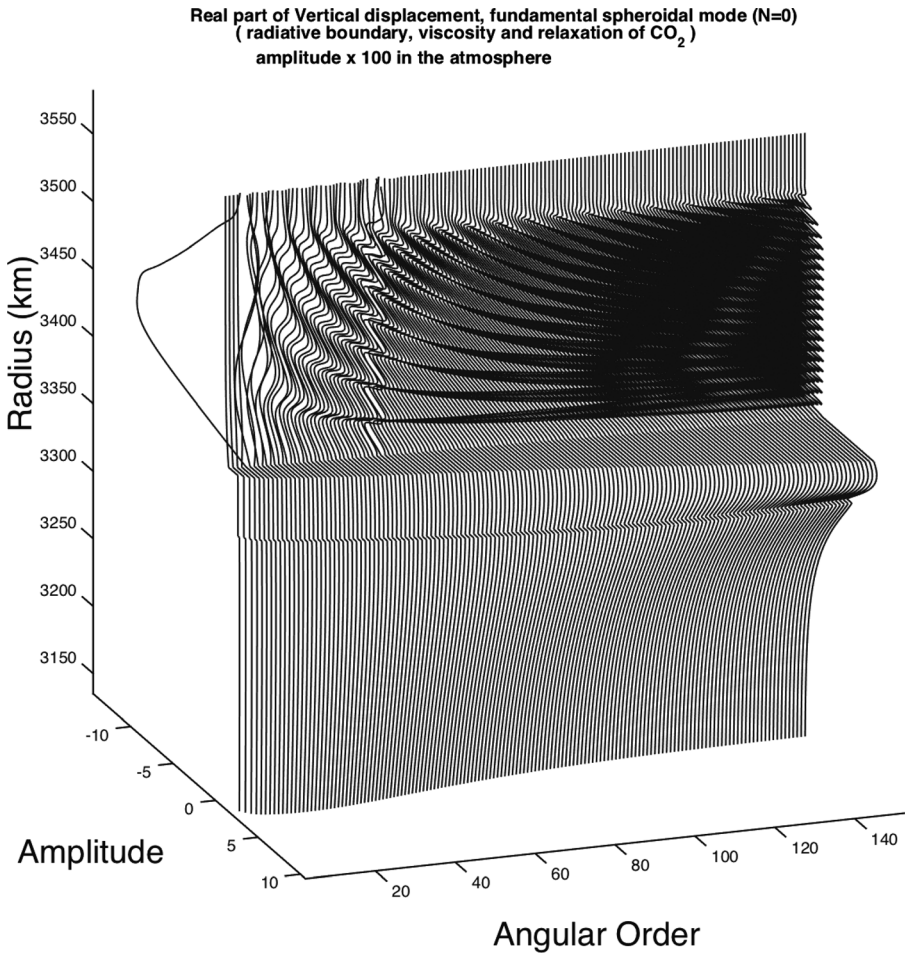

FIG. 14. Amplitudes of the vertical displacement of Rayleigh normal modes on Mars from $\ell = 0$ to $\ell = 100$, corresponding therefore to a frequency up to about 20 mHz. Note the first large resonance, for $\ell = 9$. As for Fig. 3, modes amplitude are multiplied by $\sqrt{\rho}$.

modes for models with different boundary conditions and with or without viscosity and relaxation. Although being model dependent and specific to the model used, we retrieve indeed these large resonances in amplitude when viscosity and molecular relaxation are added to the model. The resonance for these two modes generates also an increase of the amplitude, which is larger than the effect of attenuation significant only above 100 km of altitude. Further studies will be requested to confirm this counter-intuitive resonance effect and to check if the neglected terms in the wave equation are not affecting its strength.

C. Atmospheric coupling of Rayleigh modes and surface waves on Venus

Due to the much larger density of the atmosphere, Venus atmospheric coupling is exacerbated as compared to Earth. Venus appears to be the Planet where seismic waves cannot only lead to large atmospheric signals, as on Earth, but where in return the atmosphere is significantly affecting the propagation properties of surface waves in the solid planet.

We modeled Rayleigh normal modes and acoustic normal modes by using an internal Venus model based on PREM, assuming the same velocities and density profile as on Earth, as a function of pressure. The atmospheric model used was the Venus-GRAM model. Both interior and atmospheric models are shown in Fig. 10 and the atmosphere was extended up to 250 km of altitude.

Contrary to the previous modeling shown in Lognonné and Johnson (2007), Rayleigh normal modes have been computed by adding to these models the viscosity and molecular relaxation computed from the atmospheric pressure and temperature of the Venus-GRAM model with expression of Bass and Chambers (2001). This assumes pure CO_2 and is described at the beginning of Sec. V. Acoustic modes have also been computed to better understand and illustrate acoustic resonances.

As for the Earth, we retrieve indeed large peaks of resonances, for the Rayleigh modes located at the crossing of the Rayleigh branch with fundamental and overtones acoustic branches (Fig. 15). Only the fundamental and the first two overtones, with frequencies smaller than about 4.5 mHz, are trapped in the atmosphere and have Q larger than 100 for the second overtone and 1000 for the fundamental and first overtone. Only these three resonances are therefore associated to large atmospheric amplitudes for the Rayleigh waves at frequencies of about 3.1, 4.15, and 4.7 mHz, the latter being of course model dependent, with likely significant variations with local time and latitude. These three Rayleigh modes have almost equi-partition of the energy in the atmosphere, with 40%–47% of the energy in the atmosphere. An interesting feature is found in the quality factor of the fundamental and first resonances, at 3.1 and 4.15 mHz. In both cases, as shown in Fig. 15, the quality factors of the normal modes increase, from about 210 to 325 for the 3.1 mHz resonance and from 170 to 280 for the 4.15 mHz one, indicating that the

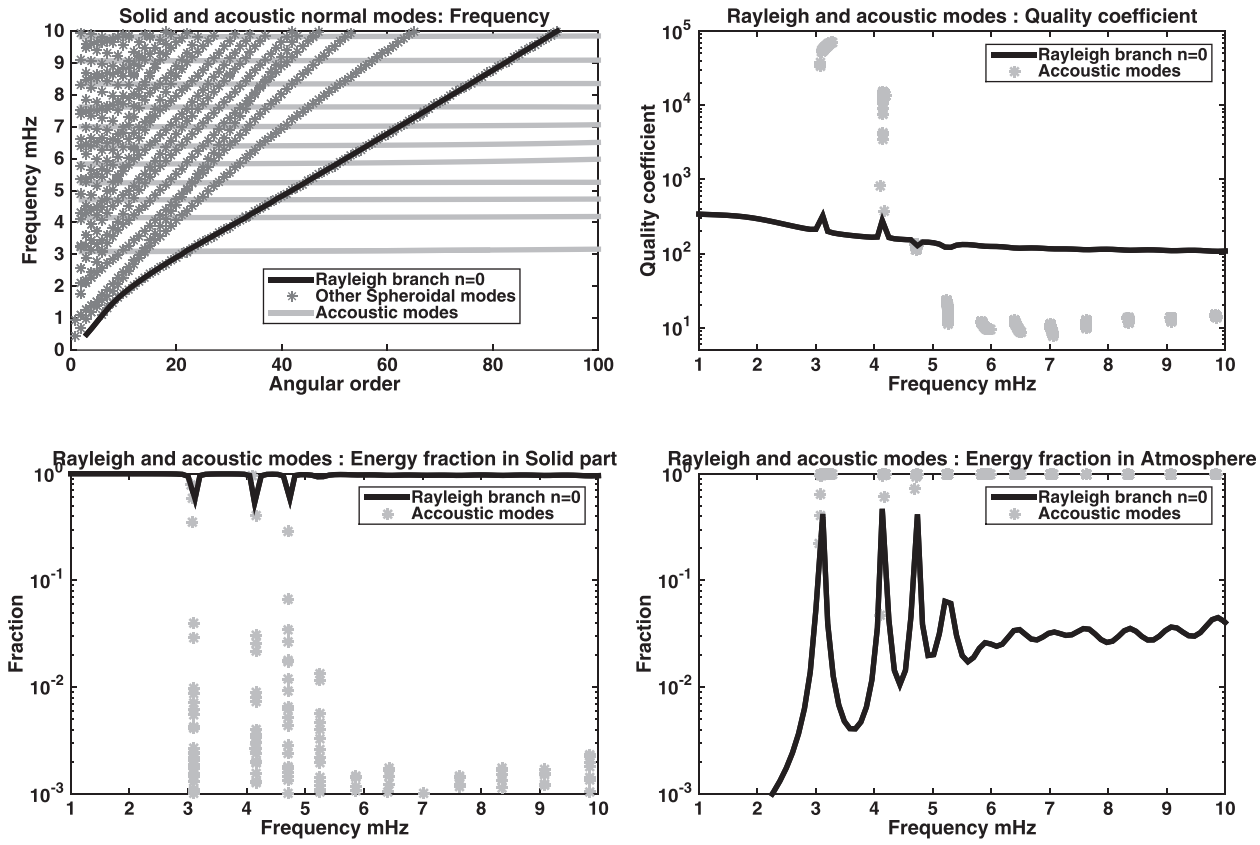

FIG. 15. Top left are the dispersion curves of fundamental Rayleigh modes (black line), together with acoustic branches (light gray) and other spheroidal solid part normal modes (dark gray). Top right shows the quality factor of both the Rayleigh modes (black line) and the acoustic modes (light gray circles). Note the large quality factor of the fundamental and first overtone, with values larger than 10^4 for the fundamental and 10^3 for the first overtone. Smaller values are found for the acoustic modes closest from the crossing with the spheroidal branch, indicating significant coupling with the solid part, especially the crust, where shear quality factors are about 600. The second and especially the third acoustic overtones are not trapped anymore and have their Q decreasing strongly from about 100 for the second to 10 or less for the third. The two bottom curves are providing the energy of the normal modes in both the solid part (bottom left) and in the atmosphere (bottom right). The bottom right shows large resonances, with almost equi-partition of the energy of the resonance modes between the atmosphere and the solid part.

propagation in the atmosphere of the Rayleigh normal modes is less attenuated than in the solid part of the planet. The quality factors used here for the solid part were those of PREM, with about 600 in the crust and ranging from 80 to about 150 in the upper mantle. At 4.7 mHz, we observe the inverse feature, with a smaller Q at the resonance, indicating this time that the lack of trapping in the atmosphere is providing a source of attenuation larger than those in the solid planet.

At larger frequencies, a weaker and last resonance is found at 5.20 mHz with about 6% of energy in the atmosphere. When comparing the amplitude of this resonance amplitude with the one modeled previously by Lognonné and Johnson (2007) without attenuation processes, we note a smaller amplitude, as a consequence of the atmospheric attenuation which reduces the energy fraction of the mode in the atmosphere and keep it closer from the continuum value, which range between 2.5% and 3.5% and is found for larger frequencies. The normal modes are shown in Figs. 16 and 17 for the real and imaginary part of the vertical amplitudes of the Rayleigh Normal modes. We retrieve the same feature as for Earth and Mars, but without that time amplification in the atmosphere and with the four resonances discussed above. Together with the horizontal amplitudes, these amplitudes can be used to compute seismograms, which will be performed in Sec. V D.

D. Observation perspectives on Venus

Today, atmospheric observations of seismic waves are done routinely on Earth, originating from the impulsive forcing above the rupture area or for surface waves at remote distances. See Lognonné (2009), Occhipinti *et al.* (2013), and Occhipinti (2015) for reviews. The most common observation techniques are GPS or Doppler as described in Sec. IV B, but red 630 nm airglow observations have been recently performed also for tsunami waves following the large, Ms = 9 Tohoku earthquake in 2011 (Makela *et al.*, 2011; Occhipinti *et al.*, 2011). But so far, no airglow observations of Rayleigh waves on Earth have been made, mainly due to the shorter period of the latter as compared to tsunamis, incompatible with the large exposure time of the airglow observations.

For Venus, only modeling have been made sofar unfortunately. Garcia *et al.* (2005) have estimated the amplitudes of temperature variations above quakes, simulating the Venus equivalent of the thermospheric heating observation made on Earth (e.g. Kelley *et al.*, 1985). Lognonné and Johnson (2007) have made a first estimation at teleseismic distances for the vertical velocities, providing a first threshold value for detection by infrared imaging and Doppler techniques, respectively. We focus here on the potential of airglow measurements.

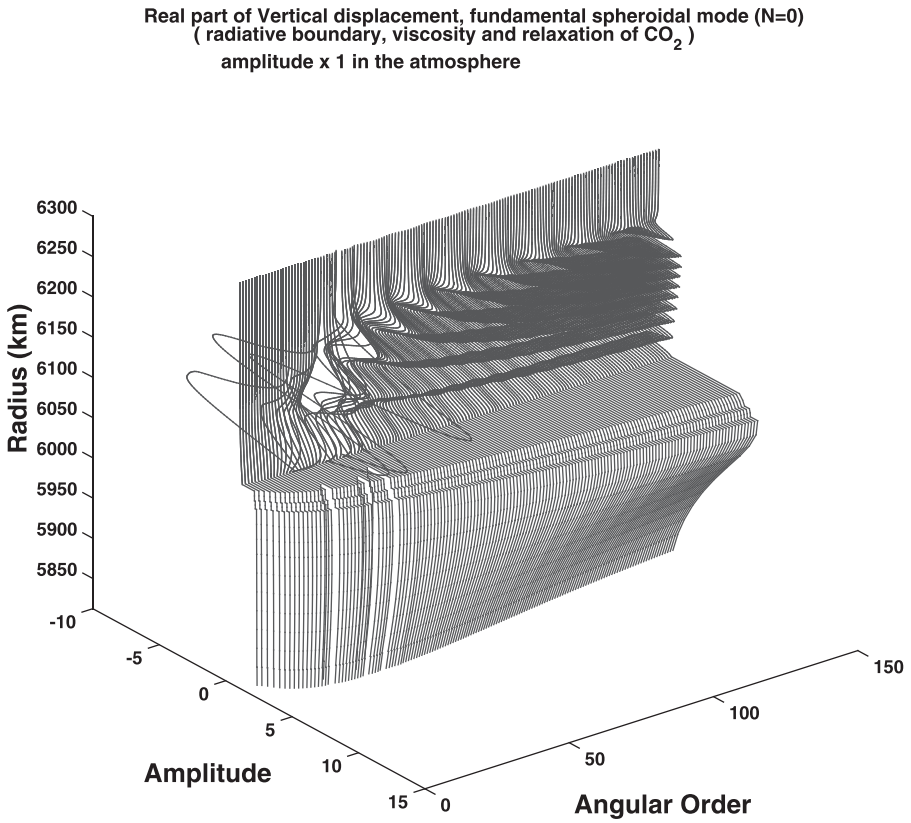

FIG. 16. Real part of the vertical amplitude of the solid spheroidal normal modes in the upper mantle and atmosphere. Fundamental modes for Venus. Same normalization as for Fig. 3.

1. Airglow estimation: Theoretical expression

Among the different airglows observed on Venus, the O2 airglow at 1.27 μm, first detected by Connes *et al.* (1979), is among the strongest one and is larger than the visible airglows by 2 orders of magnitude. It is known as the best tracer of transport of atomic oxygen (Krasnopolsky, 2011) and can therefore be targeted as a candidate for detecting the flux of atomic oxygen carried by seismic waves. Moreover,

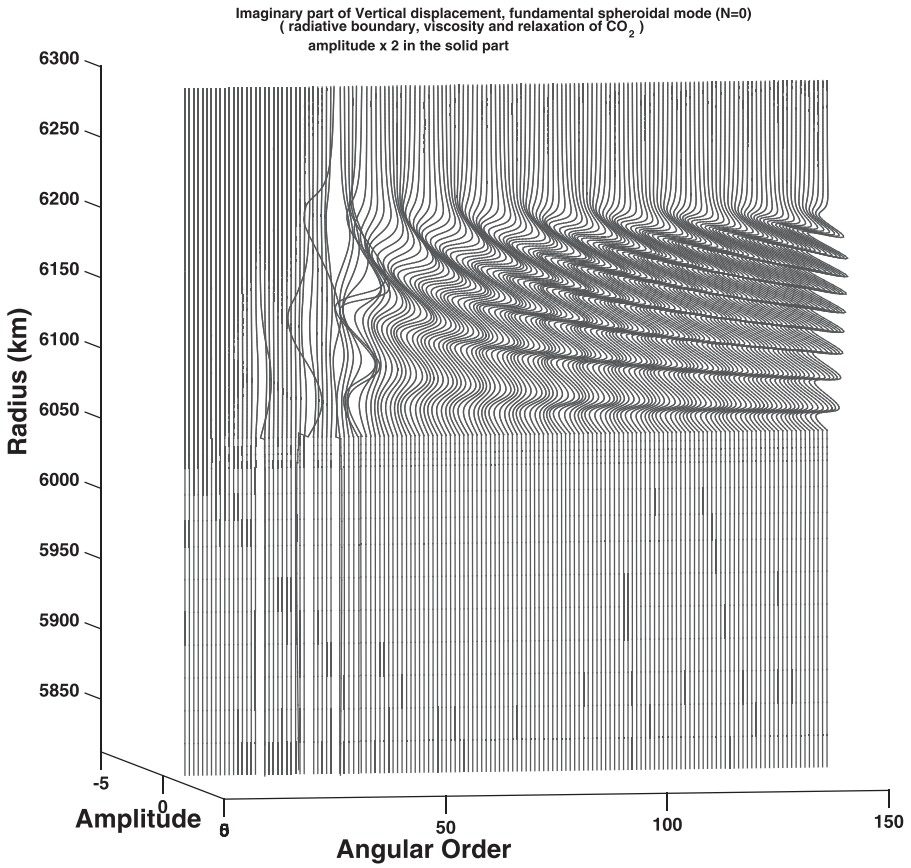

FIG. 17. Imaginary part of the vertical amplitude of the solid spheroidal normal modes in the upper mantle and atmosphere. Fundamental modes for Venus. Same normalization as for Fig. 3.

and in contrary to other nightglow [such as Herzberg I&II and Chamberlain (Krasnopolsky, 2011)], the 4460 s radiative lifetime of the 1270 μm nightglow is large and much larger than the period of the seismic waves, enabling *a priori* a nice window for the detection of time variations associated to the Rayleigh waves in the bandwidth 10–100 s.

Following the airglow theory described by Gérard *et al.* (2013) and Krasnopolsky (2011), let us consider a recombination process with a third body M

$$\mathrm{O} + \mathrm{O} + M \rightarrow \mathrm{O}_2^i + M, \tag{13}$$

where M is either CO_2 or O, and i denotes the excitation state of oxygen (namely, $a_1\Delta$ for the Infra-Red (IR) atmospheric system). The local number density of exited oxygen is given by the following equations:

$$\frac{\partial[\mathrm{O}_2^i]}{\partial t} = P - L - \nabla\cdot\left[[\mathrm{O}_2^i]\mathbf{v}\right], \tag{14}$$

$$P = \epsilon_i K[O]^2[M], \tag{15}$$

$$L = [\mathrm{O}_2^i]\left(\frac{1}{\tau_i} + k^i_{\mathrm{CO}_2}[\mathrm{CO}_2] + k^i_{\mathrm{O}}[\mathrm{O}]\right), \tag{16}$$

where $[M]$ is the total number density, [O] and $[CO_2]$ the local numbers densities of O and CO_2; ϵ_i is the net yield of the i state of O_2, τ_i is the radiative lifetime of the i state, and K is total rate coefficient of processes. $k^i_{\mathrm{CO}_2}$ and k^i_{O} are the quenching coefficients of the i state by CO_2 and O, respectively. The volume emission rate (VER) is given by

$$\mathrm{VER} = A_i[\mathrm{O}_2^i]\,. \tag{17}$$

In the steady state with no transport, $P = L$ and we get the classical VER production rate expression

$$\mathrm{VER} = \epsilon_i K[\mathrm{O}]^2[\mathrm{M}]\frac{A_i}{\frac{1}{\tau_i} + k^i_{\mathrm{CO}_2}[\mathrm{CO}_2] + k^i_{\mathrm{O}}[\mathrm{O}]}. \tag{18}$$

In the case of atmospheric perturbation by seismic waves, we will rewrite the local number of densities by adding a perturbation associated to this wave, as follows:

$$\begin{aligned}
[\mathrm{O}_2^i] &= [\mathrm{O}_2^i]_{\mathrm{eq}} + \delta[\mathrm{O}_2^i],\\
[\mathrm{O}_2] &= [\mathrm{O}_2]_{\mathrm{eq}} + \delta[\mathrm{O}_2],\\
[\mathrm{O}] &= [\mathrm{O}]_{\mathrm{eq}} + \delta[\mathrm{O}],
\end{aligned} \tag{19}$$

where the index $_{\mathrm{eq}}$ denotes the concentration at equilibrium, while those with δ are the perturbation generated by the waves. All non-excited or neutral species have their density verifying the conservation equation, and for a perturbation with an angular frequency of ω, we therefore have to first order the conservation equation

$$\frac{\partial[M]}{\partial t} + \nabla\cdot([M]\mathbf{v}) = 0, \tag{20}$$

which can be rewritten, for normal modes, as

$$\delta[M] = -\frac{\nabla\cdot([M]\mathbf{v})}{i\omega}, \tag{21}$$

where ω is the normal mode frequency. The set of equations providing the local number density of excited oxygen, always to first order and for comparable perturbation gives

$$i\omega\delta[\mathrm{O}_2^i] = \delta P - \delta L - \nabla\cdot([\mathrm{O}_2^i]\mathbf{v}), \tag{22}$$

$$\begin{aligned}
\frac{\delta P}{P} &= 2\frac{\delta[\mathrm{O}]}{[\mathrm{O}]} + \frac{\delta[M]}{[M]},\\
\frac{\delta L}{L} &= \frac{\delta[\mathrm{O}_2^i]}{[\mathrm{O}_2^i]} + [\mathrm{O}_2^i]\frac{k^i_{\mathrm{CO}_2}\delta[\mathrm{CO}_2] + k^i_{\mathrm{O}}\delta[\mathrm{O}]}{\frac{1}{\tau_i} + k^i_{\mathrm{CO}_2}[\mathrm{CO}_2] + k^i_{\mathrm{O}}[\mathrm{O}]}.
\end{aligned} \tag{23}$$

This can be used to compute the linear perturbation of any airglow and requests the chemical compositions. For the particular IR atmospheric system nightglow, the quenching coefficients have values of about $10^{-20}\mathrm{cm}^3\,\mathrm{s}^{-1}$ and $2\times10^{-16}\mathrm{cm}^3\,\mathrm{s}^{-1}$, while the local number densities are $10^{15}\,\mathrm{cm}^{-3}$ and $10^{11}\,\mathrm{cm}^{-3}$, respectively, and $1/\tau = 2\times10^{-4}\,\mathrm{s}^{-1}$. We can therefore assume, for a simplified expression of the VER perturbation, that $(1/\tau_i) + k^i_{\mathrm{CO}_2}[\mathrm{CO}_2] + k^i_{\mathrm{O}}[\mathrm{O}] = 1/\tau_i$ and divide then expression (25) by $P = L \simeq \tau_i[\mathrm{O}_2^i]$. We then get

$$\begin{aligned}
(1+\tau_i\omega)\frac{\delta[\mathrm{O}_2^i]}{[\mathrm{O}_2^i]} &\simeq 2\frac{\delta[\mathrm{O}]}{[\mathrm{O}]} + \frac{\delta[M]}{[M]} - \tau_i\frac{\nabla\cdot\left[[\mathrm{O}_2^i]\mathbf{v}\right]}{[\mathrm{O}_2^i]},\\
&\simeq -\frac{1}{i\omega}\left(2\frac{\nabla\cdot[[\mathrm{O}]\mathbf{v}]}{[\mathrm{O}]} + \frac{\nabla\cdot[[M]\mathbf{v}]}{[M]}\right)\\
&\quad -\tau_i\frac{\nabla\cdot\left[[\mathrm{O}_2^i]\mathbf{v}\right]}{[\mathrm{O}_2^i]},
\end{aligned} \tag{24}$$

which can be further simplified for 10–100 s surface waves, as $(1/\omega) \ll \tau_i$. This finally gives a simple estimation of the VER associated to wave perturbations

$$\begin{aligned}
\delta[\mathrm{VER}] = A_i\delta[\mathrm{O}_2^i] &= -\frac{A_i\tau_i}{1+\tau_i\omega}\nabla\cdot\left[[\mathrm{O}_2^i]\mathbf{v}\right]\\
&= -\frac{\tau_i}{1+\tau_i\omega}\nabla.[[\mathrm{VER}]\mathbf{v}].
\end{aligned} \tag{25}$$

The perturbation of VER appears therefore to be the transported VER by the wind generated by the Rayleigh waves multiplied by a low pass filter with time constant τ_i.

2. Airglow estimation: Modeling for quakes

Based on the observed O_2 VER fluxes observed with VIRTIS (Gérard *et al.*, 2013), we performed the modeling of the signal associated to a 6.5 Venus Quake. Simulation has been done by a full modeling of the Rayleigh seismic waves for a Venus-GRAM atmospheric model taking into account all dissipation effects, including molecular relaxation, as described in Sec. V A. With that respect, we have computed the time variations of the VER generated by Rayleigh waves from Eq. (25). The vertical profile of the VER used in

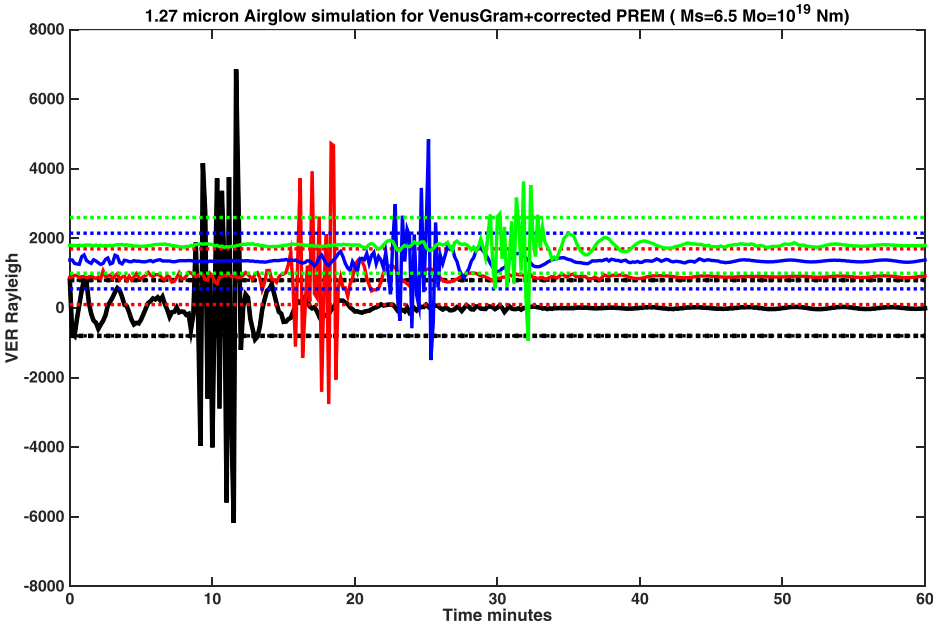

FIG. 18. (Color online) Simulation of the VER generated by an Ms = 6.5 quake, at several epicentral distances, assuming 9 s of integration. Seismograms are low pass filtered at 0.04 Hz. Amplitudes have a SNR larger than 2 for the 1600 Rayleigh detection threshold (threshold dashed line) up to 60° of epicentral distance by an increment of 15°. Each airglow synthetic emission rate is shifted by 30 (Δ-15), where Δ is the epicentral distance. Solid part is PREM for the upper mantle (as a function of pressure) and crust with $Qs = 600$, but with the Venus radius and a Venus core fitting the Venus mass. Atmospheric model is Venus Gram.

Eq. (25) is the one proposed by Krasnopolsky (2011). It corresponds to the O_2 nightglow at 1.27 μm with quenching by CO_2 and CO [Profile (2) of Fig. 3 from Krasnopolsky (2011)]. We refer the reader to this paper for more details on the different terms, compositions, and parameters enabling the computation of this VER profile. The Rayleigh wave generated atmospheric winds are obtained from the Venus Rayleigh normal modes summation and are computed for all altitudes. The VER perturbation has then been vertically integrated in order to observe the full emission of the atmospheric column of the atmospheric area expected to be observed and is expressed in Rayleigh. Normal modes frequencies allows to compute exactly Eq. (25) for each individual Normal mode contribution, but as the time constant τ is much larger than the periods of the most energetic normal modes, the low pass filter can practically be assumed to be a perfect integrator and the perturbation can then be obtained directly from the atmospheric displacement of the atmosphere computed by the normal modes summation.

These simulations provide the atmospheric emission potentially observed from a satellite in Medium Venus Orbit (e.g., relatively far from the planet and at several 10 000 km). This demonstrates that a magnitude 6.5 (with strike, dip, and rake all equal 45° and depth of 30 km) can be observed by existing infrared remote sensing instruments. One possibility might be the instrument onboard VERITAS, a Discovery proposal selected recently by NASA for STEP1 (Smrekar *et al.*, 2014), if of course the latter has a dedicated airglow filter at 1.27 μm. Signals up to 60° of epicentral distance with a signal-to-noise ratio (SNR) greater than 2 at the pixel level, large enough for all further processing necessary for the measurement of the phase or group velocity of the seismic waves can be expected, as seen in Fig. 18.

VI. DISCUSSION AND CONCLUSION

In the last 15 yrs, observations and modeling of Rayleigh surface waves in the Earth atmosphere have reached maturity. Comparable observations of course remain to be done on other planets, but we can however expect this to be the case in the next decade. On Mars, the NASA InSight mission will indeed deploy by 2018 a seismometer and an infrasonic pressure sensor, enabling the monitoring of air-coupled seismic waves. Much remains to be done for fully estimating their amplitude, but we can likely consider that Rayleigh waves generated by the airburst from impacts might be detected, as rates estimated to about five seismic events per year (Lognonné and Kawamura, 2015). This will be developed furthermore in future works.

The deployment of a long duration geophysical station on Venus will however be much more challenging, due to both the high pressure and temperature at the surface. But as shown in Sec. V, the remote detection of seismic waves through airglow observation might be envisaged from orbit. Some estimates of the Venus activity were done for the past Venus Internal Structure Mission NASA Discovery proposal (Stofan *et al.*, 1993). The range of seismicity is pretty wide, depending on the source of strain accumulation and on the thickness assumed for the seismogenic layer. By assuming a layer thickness of 30 km, based on heat flow estimates and a strain rate of 10^{-19} s^{-1}, an activity of 25 quakes per year with moment magnitude larger than 6 and 125 quakes per year with moment larger than 5 was proposed. This will be enough to achieve the detection of a few quakes per year up to 60° of epicentral distance for remote sensing instrument with a 1600 Rayleigh threshold, and much more if future instruments can be developed with a smaller detection threshold.

ACKNOWLEDGMENTS

This work has been supported by the French Space Agency CNES in the frame of the InSight/SEIS Mars mission and by the Institut Universitaire de France and CNES for the Veritas Venus project. F.K. acknowledges the financial support of the UnivEarthS Labex program at

Sorbonne Paris Cité (ANR-10-LABX-0023 and ANR-11-IDEX-0005-02) and of the SODERN company for his Ph.D. support. The recent development of the Earth's atmospheric coupling software in IPGP was partially supported by the U.S. Office of Naval Research through the TWIST project (N000141310035). We thank W. B. Banerdt and S. Smrekar, both at the Jet Propulsion Laboratory for their promotion of Planetary seismology onboard NASA Mission projects. Part of this work benefited from support of the Keck Institute for Space Studies at CalTech, and we thank C. Sotin, J. Cutts, R. Garcia, and D. Mimoun for fruitful discussions. We also thank G. Occhipinti and an anonymous reviewer for their constructive reviews. This is IPGP contribution 3756.

Aki, K., and Richards, P. G. (**1980**). *Quantitative Seismology* (Freeman, San Francisco, CA).

Artru, J., Farges, T., and Lognonné, P. (**2004**). "Acoustic waves generated from seismic surface waves: Propagation properties determined from Doppler sounding observation and normal-modes modeling," Geophys. J. Int. **158**, 1067–1077.

Artru, J., Lognonné, P., and Blanc, E. (**2001**). "Normal modes modelling of post-seismic ionospheric oscillations," Geophys. Res. Lett. **28**(4), 697–700, doi:10.1029/2000GL000085.

Astafyeva, E., and Heki, K. (**2009**). "Dependence of waveform of nearfield co-seismic ionospheric disturbances on focal mechanisms," Earth Planets Space **61**, 939–943.

Astafyeva, E., Heki, K., Kiryushkin, V., Afraimovich, E., and Shalimov, S. (**2009**). "Two mode long distance propagation of coseismic ionosphere disturbances," J. Geophys. Res. **114**, A10307, doi:10.1029/2008JA013853.

Bass, H., and Chambers, J. (**2001**). "Absorption of sound in the Martian atmosphere," J. Acoust. Soc. Am. **109**, 3069–3071.

Ben-Menahem, A. (**1975**). "Source parameters of the Siberian explosion of June 30, 1908, from analysis and synthesis of seismic signal at four stations," Phys. Earth Planet. Int. **11**, 1–35.

Borovička, J., Spurny, P., Brown, P., Wiegert, P., Kalenda, P., Clark, D., and Shrbeny, L. (**2013**). "The trajectory, structure and origin of the Chelyabinsk asteroidal impactor," Nature **503**(7475), 235–237.

Bourdillon, A., Occhipinti, G., Molinie, J.-P., and Rannou, V. (**2014**). "HF radar detection of infrasonic waves generated in the ionosphere by the 28 March 2005 Sumatra earthquake," J. Atmos. Sol.-Terr. Phys. **109**, 75–79.

Brissaud, Q., Martin, R., Garcia, R. F., and Komatitsch, D. (**2016**). "Finite-difference numerical modelling of gravitoacoustic wave propagation in a windy and attenuating atmosphere," Geophys. J. Int. **206**, 308–327.

Calais, E., and Minster, J. B. (**1995**). "GPS detection of ionospheric perturbations following the January 17, 1994, Northridge earthquake," Geophys. Res. Lett. **22**, 1045–1048, doi:10.1029/95GL00168.

Chum, J., Hruska, F., Zednik, J., and Lastovicka, J. (**2012**). "Ionospheric disturbances (infrasound waves) over the Czech Republic excited by the 2011 Tohoku earthquake," J. Geophys. Res. **117**, A08319, doi:10.1029/2012JA017767.

Connes, P., Noxon, J. F., Traub, W. A., and Carleton, N. P. (**1979**). "O2(1D) emission in the day and night airglow of Venus," Astrophys. J. **233**, L29–L32.

Davis, K., and Baker, D. M. (**1965**). "Ionospheric effects observed around the time of the Alaskan earthquake of March 28, 1964," J. Geophys. Res. **70**, 1251–1253, doi:10.1029/JZ070i009p02251.

Donn, W. L., and Ewing, M. (**1962a**). "Atmospheric waves from nuclear explosions," J. Geophys. Res. **67**, 1855–1866, doi:10.1029/JZ067i005p01855.

Donn, W. L., and Ewing, M. (**1962b**). "Atmospheric waves from nuclear explosion. 2. The Soviet test of October 30, 1961," J. Atmos. Sci. **19**, 264–273.

Ducic, V., Artru, J., and Lognonné, P. (**2003**). "Ionospheric remote sensing of the Denali Earthquake Rayleigh surface waves," Geophys. Res. Lett. **30**(18), 1951, doi:10.1029/2003GL017812.

Dziewonski, A. M., and Anderson, D. L. (**1981**). "Preliminary reference Earth model," Phys. Earth Planet. Inter. **25**, 297–356.

Edwards, W. N. (**2008**). "Meteor generated infrasound: Theory and observation," in *Infrasound Monitoring for Atmospheric Studies*, edited by A. Le Pichon (Springer-Verlag, New York), Chap. 12, pp. 355–408.

Edwards, W. N., Eaton, D. W., and Brown, P. G. (**2008**). "Seismic observations of meteors: Coupling theory and observations," Rev. Geophys. **46**, RG4007, doi:10.1029/2007RG000253.

Forget, F., Hourdin, F., Fournier, R., Hourdin, C., Talagrand, O., Collins, M., Lewis, S. R., Read, P. L., and Huot, J.-P. (**1999**). "Improved general circulation models of the Martian atmosphere from the surface to above 80 km," J. Geophys. Res. **104**, 24155–24176, doi:10.1029/1999JE001025.

Francis, S. H. (**1973**). "Acoustic-gravity modes and large-scale traveling ionospheric disturbances of a realistic, dissipative atmosphere," J. Geophys. Res. **78**, 2278–2301, doi:10.1029/JA078i013p02278.

Fukao, Y., Nishida, K., Suda, N., Nawa, K., and Kobayashi, N. (**2002**). "A theory of the Earth's background free oscillations," J. Geophys. Res. **107**, 11-1–11-11, doi:10.1029/2001JB000153.

Garcia, R., Crespon, F., Ducic, V., and Lognonné, P. (**2005**). "Three-dimensional ionospheric tomography of post-seismic perturbations produced by the Denali earthquake from GPS data," Geophys. J. Int. **163**, 1049–1064, doi:10.1111/j.1365-246X.2005.02775.x.

Garcia, R., Lognonné, P., and Bonnin, X. (**2005**). "Detecting atmospheric perturbations produced by Venus quakes," Geophys. Res. Lett. **32**, L16205, doi:10.1029/2005GL023558.

Garcia, R. F., Bruinsma, S., Lognonné, P., Doornbos, E., and Cachoux, F. (**2013**). "GOCE: The first seismometer in orbit around the Earth," Geophys. Res. Lett. **40**, 1015–1020, doi:10.1002/grl.50205.

Gérard, J. C., Soret, L., Migliorini, A., and Piccioni, G. (**2013**). "Oxygen nightglow emissions of Venus: Vertical distribution and collisional quenching," Icarus **223**, 602–608.

Harkrider, D. G. (**1964**). "Theoretical and observed acoustic-gravity waves from explosive sources in the atmosphere," J. Geophys. Res. **69**, 5295–5321, doi:10.1029/JZ069i024p05295.

Hunt, J. N., Palmaer, R., and Penney, Sir W. (**1960**). "Atmospheric waves caused by large explosions," Phil. Trans. R. Soc. London A **43**, 17–34.

Kanamori, H., and Mori, J. (**1992**). "Harmonic excitation of mantle Rayleigh waves by the 1991 eruption of mount Pinatubo, Philippines," Geophys. Res. Lett. **19**, 721–724, doi:10.1029/92GL00258.

Kanamori, H., Mori, J., and Harkrider, D. G. (**1994**). "Excitation of atmospheric oscillations by volcanic eruptions," J. Geophys. Res. **22**, 947–961.

Kelley, M. C., Livingston, R., and McCready, M. (**1985**). "Large amplitude thermospheric oscillations induced by an earthquake," Geophys. Res. Lett. **12**, 577–580, doi:10.1029/GL012i009p00577.

Kobayashi, N. (**2007**). "A new method to calculate normal modes," Geophys. J. Int. **168**, 315–331.

Kobayashi, N., and Nishida, K. (**1998a**). "Continuous excitation of planetary free oscillations by atmospheric disturbances," Nature **395**, 357–360.

Kobayashi, N., and Nishida, K. (**1998b**). "Atmospheric excitation of planetary free oscillations," J. Phys. Condens. Matter **10**, 11557–11560.

Krasnopolsky, V. A. (**2011**). "Excitation of the oxygen nightglow on the terrestrial planets," Planet. Space Sci. **59**, 754–766.

Leonard, R. S., and Barnes, R. A., Jr. (**1965**). "Observation of ionospheric disturbances following the Alaska earthquake," J. Geophys. Res. **70**, 1250–1253, doi:10.1029/JZ070i005p01250.

Lognonné, P. (**1991**). "Normal modes and seismograms of an anelastic rotating Earth," J. Geophys. Res. **96**, 20309–20319, doi:10.1029/91JB00420.

Lognonné, P. (**2005**). "Planetary seismology," Ann. Rev. Earth Planet. Sci. **33**, 571–604.

Lognonné P. (**2009**). "Seismic waves from atmospheric sources and Atmospheric-Ionospheric signatures of seismic waves," in *Infrasound Monitoring for Atmospheric Studies*, edited by A. Le Pichon (Springer-Verlag, New York), Chap. 10, pp. 281–304.

Lognonné, P., Artru, J., Garcia, R., Crespon, F., Ducic, V., Jeansou, E., Occhipinti, G., Helbert, J., Moreaux, G., and Godet, P.-E. (**2006**). "Ground based GPS tomography of ionospheric post-seismic signal," Planet. Space Sci. **54**, 528–540.

Lognonné, P., Clévédé, C., and Kanamori, H. (**1998**). "Normal mode summation of seismograms and barograms in an spherical Earth with realistic atmosphere," Geophys. J. Int. **135**, 388–406.

Lognonné P., and Clévédé, E. (**2002**). "Normal modes of the Earth and Planets," *Handbook on Earthquake and Engineering Seismology*, International Geophysics series, 81A, 125–147, IASPEI Centennial Publications, edtied by W. H. K. Lee, H. Kanamori, P. C. Jennings, and C. Kisslinger (Academic Press, San Diego), Chap. 10.

Lognonné P., and Johnson, C. (**2007**). "Planetary seismology," in *Treatrise in Geophysics*, Planets and Moons, edited by G. Shubert (Elsevier, New York), Vol. 10, Chap. 4, pp. 69–122.
Lognonné, P., and Kawamura, T. (**2015**). "Impact seismology on terrestrial and giant planets," in *Extraterrestrial Seismology*, edited by V. Tong and R. Garcia (Cambridge University Press, London), Chap. 20, pp. 250–263.
Lognonné, P, Mosser, B., and Dahlen, F. A. (**1994**). "Excitation of the Jovian seismic waves by the Shoemaker-Levy 9 cometary impact," Icarus **110**, 186–195.
Makela, J. J., Lognonné, P., Hébert, H., Gehrels, T., Rolland, L., Allgeyer, S., Kherani, A., Occhipinti, G., Astafyeva, E., Coisson, P., Loevenbruck, L., Clévédé, E., Kelley, M. C., and Lamouroux, J. (**2011**). "Imaging and modeling the ionospheric airglow response over Hawaii to the tsunami generated by the Tohoku Earthquake of 11 March 2011," Geophys. Res. Lett. **38**, L00G02, doi:10.1029/2011GL047860.
Maruyama, T., and Shinagawa, H. (**2014**). "Infrasonic sounds excited by seismic waves of the 2011 Tohoku-oki earthquake as visualized in ionograms," J. Geophys. Res. Space Phys. **119**, 4094–4108, doi:10.1002/2013JA019707.
Maruyama, T., Tsugawa, T., Kato, H., Ishii, M., and Nishioka, M. (**2012**). "Rayleigh wave signature in ionograms induced by strong earthquakes," J. Geophys. Res. **117**, A08306, doi:10.1029/2012JA017952.
Master, G., Barmine, M., and Kientz, S (**2014**). *Mineos user Manual*, version 1.0.2, https://geodynamics.org/cig/software/mineos/ (Last viewed 8/21/2016).
Mutschlechner, J. P., and Whitaker, R. W. (**2009**). "Some atmospheric effects on infrasound signal amplitudes," in *Infrasound Monitoring for Atmospheric Studies*, edited by A. Le Pichon (Springer-Verlag, New York), Chap. 14, pp. 475–507.
Myers, S. C., Begnaud, M. L., Ballard, S., Pasyanos, M. E., Phillips, W. S., Ramirez, A. L., Antolik, M. S., Hutchenson, K. D., Wagner, G. S., Dwyer, J. J., Rowe, C. A., and Russell, D. R. (**2010**). "A crust and upper mantle model of Eurasia and North Africa for Pn travel time calculation," Bull. Seism. Soc. Am. **100**(2), 640–656.
Nawa, K., Suda, N., Fukao, Y., Sato, T., Aoyama, Y., and Shibuya, K. (**1998**). "Incessant excitation of the Earth's free oscillations," Earth Planet. Space **50**, 3–8.
Nishida, K. (**2013**). "Earth's background free oscillations," Ann. Rev. Earth Planet. Sci. **41**, 719–740.
Nishida, K. (**2014**). "Source spectra of seismic hum," Geophysical J. **199**, 416–429.
Nishida, K., and Kobayashi, N. (**1999**). "Statistical features of Earth's continuous free oscillations," J. Geophys. Res. **104**, 28741–28750, doi:10.1029/1999JB900286.
Nishida, K., Kobayashi, N., and Fukao, Y. (**2000**). "Resonant oscillations between the solid Earth and the Atmosphere," Science **287**, 2244–2246.
Occhipinti, G. (**2015**). "The seismology of the planet Mongo: The 2015 ionospheric seismology review," in *Subduction Dynamics: From Mantle to Mega Disasters*, edited by G. Morra, D. A. Yuen, S. King, S. M. Lee, and S. Stein (Wiley, New York), ISBN 978-1-118-88885-8.
Occhipinti, G., Coisson, P., Makela, J. J., Allgeyer, S., Kherani, A., Hébert, H., and Lognonné, P. (**2011**). "Three-dimensional numerical modeling of tsunami-related internal gravity waves in the Hawaiian atmosphere," Earth Planet. Sci. **63**, 847–851.
Occhipinti, G., Dorey, P., Farges, T., and Lognonné, P. (**2010**). "Nostradamus: The radar that wanted to be a seismometer," Geophys. Res. Lett. **37**, L18104, doi:10.1029/2010GL044009.
Occhipinti, G., Rolland, L., Lognonné, P., and Watada, S. (**2013**). "From Sumatra 2004 to Tohoku-Oki 2011: The systematic GPS detection of the ionospheric signature induced by tsunamigenic earthquakes," J. Geophys. Res. **118**, 3626–3636, doi:10.1002/jgra.50322.
Okal, E., and Anderson, D. J. (**1978**). "Theoretical models for Mars and their seismic properties," Icarus **33**, 514–528.
Picone, J., Hedin, A., Drob, D., and Aikin, A. (**2002**). "NRLMSISE00 empirical model of the atmosphere: Statistical comparisons and scientific issues," J. Geophys. Res. **107**(A12), 1468.
Pitteway, M. L. V., and Hines, C. O. (**1963**). "The viscous damping of atmospheric gravity waves," Can. J. Phys. **41**, 1935–1948.
Press, F., and Harkrider, D. (**1962**). "Propagation of acoustic-gravity waves in the atmosphere," J. Geophys. Res. **67**, 3889–3908, doi:10.1029/JZ067i010p03889.
Reddy, C. D., and Seemala, G. K. (**2015**). "Two-mode ionospheric response and Rayleigh wave group velocity distribution reckoned from GPS measurement following Mw 7.8 Nepal earthquake on 25 April 2015," J. Geophys. Res. Space Phys. **120**, 7049–7059.
ReVelle, D. O. (**1974**). "Acoustic of meteors effects of the atmospheric temperature and wind structure on the sounds produced by meteors," Ph.D. dissertation, University of Michigan, Ann Arbor, Michigan.
Rhie, J., and Romanowicz, B. (**2004**). "Excitations of the Earth's incessant free oscillation by atmosphere/ocean/solid Earth coupling," Nature **431**, 552–556.
Rhie, J., and Romanowicz, B. (**2006**). "A study of the relation between ocean storms and the Earth's hum," Geochem. Geophys. Geosyst. **7**(10), CiteID Q10004, doi:10.1029/2006GC001274.
Rolland, L. M., Lognonné, P., Astafyeva, E., Kherani, E. A., Kobayashi, N., Mann, M., and Munekane, H. (**2011a**). "The resonant response of the ionosphere imaged after the 2011 Tohoku-Oki earthquake," Earth Planet. Sci. **63**, 853–857.
Rolland, L. M., Lognonné, P., and Munekane, H. (**2011b**). "Detection and modeling of Rayleigh waves induced patterns in the ionosphere," J. Geophys. Res. **116**, A05320, doi:10.1029/2010JA016060.
Smrekar, S. E., Elkins-Tanton, L. T., Hensley, S., Campbell, B. A., Gilmore, M. S., Phillips, R. J., and Zebker, H. A. (**2014**). "VERITAS: A mission to study the highest priority Decadal Survey questions for Venus," American Geophysical Union, Fall Meeting 2014, Abstract P21B-3912.
Stofan, E. R., Saunders, R. S., Senske, D., Noco, K., Tralli, D., and Lundgren, P. (**1993**). "Venus interior structure mission (VISM): Establishing a seismic network on Venus," in *Workshop on Advanced Technologies for Planetary Instruments*, Part 1, 2324 pp., SEE N93-28764 1191, Lunar and Planetary Institute, Houston, TX.
Suda, N., Nawa, K., and Fukao, Y. (**1998**). "Incessant excitation of the Earth's free oscillations," Science **279**, 2089–2091.
Takeuchi, H., and Saïto, H. (**1972**). "Seismic surface waves," in *Methods in Computational Physics*, edited by B. A. Bolt (Academic Press, New York), Vol. 11, pp. 217–295.
Tanimoto, T. (**1999**). "Excitation of normal modes by atmospheric turbulence: Source of long period seismic noise," Geophys. J. Int. **136**, 395–402.
Tanimoto, T. (**2005**). "The oceanic excitation hypothesis for the continuous oscillations of the Earth," Geophys. J. Int. **160**, 276–288, doi:10.1111/j.1365-246X.2004.02484.x.
Tanimoto, T., and Um, J. (**1999**). "Cause of continuous oscillations," J. Geophys. Res. **104**, 28723–28739, doi:10.1029/1999JB900252.
Tanimoto, T., Um, J., Nishida, K., and Kabayashi, N. (**1998**). "Earth's continuous oscillations observed on seismically quiet days," Geophys. Res. Lett. **25**(10), 1553–1556, doi:10.1029/98GL01223.
Tauzin, B., Debayle, E., Quantin, C., and Coltice, N. (**2013**). "Seismoacoustic coupling induced by the breakup of the 15 February 2013 Chelyabinsk meteor," Geophys. Res. Lett. **40**, 3522–3526, doi:10.1002/grl.50683.
Unno, W., Osaki, Y., Ando, H., Saito, H., and Shibayashi, H. (**1989**). *Non-radial Oscillations of Stars* (Tokyo University Press, Japan).
Venus GRAM model, https://software.nasa.gov/software/MFS-32314-1 (last viewed 8/21/2016).
Watada, S. (**1995**). "Part 1: Near-source acoustic coupling between the atmosphere and the solid Earth during volcanic eruptions," Ph.D. thesis, California Institute of Technology, Pasadena, California.
Watada, S., and Kanamori, H. (**2010**). "Acoustic resonant oscillations between the atmosphere and the solid Earth during the 1991 Mt. Pinatubo eruption," J. Geophys. Res. **115**, B12319, doi:10.1029/2010JB007747.
Weaver, P. F., Yuen, P. C., Prolss, G. W., and Furumoto, A. S. (**1970**). "Acoustic coupling in the ionosphere from seismic waves of the earthquake at Kurile Islands on August 11, 1969," Nature **226**, 1239–1241.
Webb, S. C. (**2007**). "The Earth's 'Hum' is driven by ocean waves over the continental shelves," Nature **445**, 754–756.
Widmer, R., and Zürn, W. (**1992**). "Bichromatic excitation of long-period Rayleigh and air waves by the mount Pinatubo and El Chichon volcanic eruptions," Geophys. Res. Lett. **19**, 765–768, doi:10.1029/92GL00685.
Williams, J. P. (**2001**). "Acoustic environment of the Martian surface," J. Geophys. Res. **106**(E3), 5033–5041, doi:10.1029/1999JE001174.

Woodhouse, J. H., and Dahlen, F. A. (**1978**). The effect of a general aspherical perturbation on the free oscillations of the Earth, Geophys. J. R. Astr. Soc. **53**, 335–354.
Yamamoto, R. (**1955**). "The microbarographic oscillations produced by the explosions of hydrogen bombs in the Marshall Islands," Bull. Am. Meteorol. Soc. **37**, 406–409.
Yamamoto, R. (**1957**). "A dynamical theory of micro-barographic oscillations produced by the explosions of hydrogen bombs," J. Meteorol. Soc. Japan **35**, 32–40.
Yuen, P. C., Weaver, P. F., Suzuki, R. K., and Furumoto, A. S. (**1969**). "Continuous traveling coupling between seismic waves and the ionosphere evident in May 1968 Japan earthquake data," J. Geophys. Res. **74**, 2256–2264, doi:10.1029/JA074i009p02256.
Zürn, W., and Widmer, R. (**1996**). "Worldwide observation of bichromatic long-period Rayleigh-waves excited during the June 15, 1991 Eruption of Mt. Pinatubo," in *Fire and Mud, Eruptions of Mount Pinatubo, Philippines*, edited by C. Newhall and R. Punongbayan (University of Washington Press, Washington), pp. 615–624.